

BEN-GURION UNIVERSITY OF THE NEGEV
FACULTY OF ENGINEERING SCIENCES
DEPARTMENT OF BIOMEDICAL ENGINEERING

Duty ratio of cooperative molecular motors

Thesis submitted in partial fulfillment of the requirements for the M.Sc. degree

By: Nadiv Dharan

September, 2012

September, 2012

BEN-GURION UNIVERSITY OF THE NEGEV
FACULTY OF ENGINEERING SCIENCES
DEPARTMENT OF BIOMEDICAL ENGINEERING

Duty ratio of cooperative molecular motors

Thesis submitted in partial fulfillment of the requirements for the M.Sc. degree

By: Nadiv Dharan

Supervised by: Prof. Oded Farago

Author:.....

Date:.....

Supervisor:.....

Date:.....

Chairman of Graduate Studies Committee:.....Date:.....

September, 2012

Abstract

Motor proteins are specialized molecules that convert chemical energy into useful mechanical work and govern many important biological processes. They bind to actin filaments and microtubules and use them as tracks, on which they propagate in order to transport different types of cargo across the cell. Among these molecules we find myosin II motors that interact with elastic actin filaments. Myosin II are non processive motors that exhibit a low duty ratio, which means that in order to work effectively they need to cooperate with each other. The collective work of myosin II motors on elastic actin tracks suggests that these filaments may be subjected to significant tensile stresses. It has been found that the stress applied on the actin may induce an indirect crosstalk between the motors in order to diminish the elastic energy, which is expressed by changes in their binding / unbinding statistics. This type of indirect communication between motors via the elastic track, which has been termed the elasticity mediated crosstalk (EMC) effect, may significantly affect the motors' effective processivity. In this thesis, we use a statistical mechanical analysis and Monte Carlo computer simulations, to explore the magnitude and role of the EMC effect in two types of systems where the collective action of myosin II motors on actin filament is present: (i) gliding motility assays and (ii) muscle contraction. In motility assays, we find that the EMC effect has a small impact on the collective action of motors, and that the duty ratio of the motors remains effectively unchanged. In muscle contraction, where the actin filament is subjected to an external force opposing the action of the motors, we find that the EMC effect leads to a non uniform attachment probability along the actin track. Such duty ratio variations between motors may have a serious negative influence on the ability of the motors to perform effectively. Nevertheless, we find that this feature becomes significant only when the size of the system is larger than the size of the sarcomere (which is the basic contractile unit of the muscle cell). The EMC effect may, thus, serve as an explanation for the specific dimensions of the sarcomere, which are found to be essentially identical across different vertebrate species.

Acknowledgments

I wish to thank my supervisor, Prof. Oded Farago, for all the guidance, support and assistance throughout my thesis project.

A special thanks to my lab colleagues Noam Weil and Yotam Avital for all the assistance and useful discussions we had over the past two years.

Contents

1	Introduction	7
1.1	The cytoskeleton	7
1.2	Motors proteins	9
1.3	Cooperativity between motor proteins	11
1.3.1	Motility assays	12
1.3.2	Skeletal muscles	13
1.4	Cooperative bidirectional motion	15
1.5	The elasticity-mediated crosstalk (EMC) effect	18
1.5.1	System model	19
1.5.2	Calculating the elastic energy	20
1.5.3	The dimensionless parameter β^*	22
1.5.4	Stress fluctuations	23
1.6	Outline	24
2	The EMC effect in gilding motility assays	26
2.1	Statistical-mechanical analysis	27
2.2	Gliding assay computer simulations	31
2.3	Actin-Myosin II systems	33
2.4	Summary	34
3	The EMC effect in muscle contraction	36
3.1	Muscle contraction models	37
3.2	A simple derivation of Hill's equation	42
3.3	System model	44
3.4	Monte Carlo computer simulations	45

3.4.1	A Polarized attachment probability due to the EMC effect	46
3.4.2	Sarcomere shortening simulations	47
3.5	Summary	50
4	Discussion	52

Chapter 1

Introduction

1.1 The cytoskeleton

The cytoskeleton is a protein scaffold present in all biological cells, which serves as a supporting infrastructure that gives the cell its morphology and mechanical stability. The cytoskeleton (see Fig. 1.1) is a dynamic structure which has many important functions, such as cell shape maintenance, cellular locomotion and intracellular cargo transport [1].

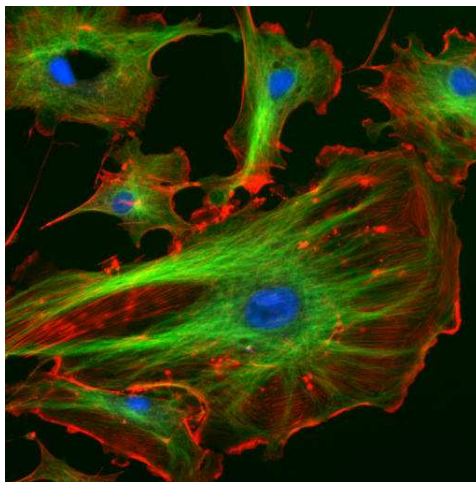


Figure 1.1: The cytoskeleton of endothelial cells showing actin filaments (red), microtubules (green) and the nuclei (blue).

Three main protein filaments compose the cytoskeleton: microtubules, actin filaments

and intermediate filaments (see Fig. 1.2). The thickest and most rigid filaments are microtubules, which are hollow, pipe-like filaments. The cylindrical structure of microtubules is made of 13 circularly arranged protofilaments, each made of successive units of α - and β -tubulin dimers [2]. The successive assembly of tubulin dimers into microtubules defines its polarity, where the “plus” and “minus” ends are at the fast and slow growing ends of the filament respectively. The rigid microtubules provide the cell important mechanical support and have a key role in intracellular transport [3, 4], cell division [5] and other important cellular processes. Actin filaments, whose diameter is ~ 7 nm, are the thinnest filaments of the cytoskeleton. Actin filaments are relatively flexible cable-like filaments, with a double helical structure repeating every ~ 38 nm, composed of G-actin monomers. Actin filaments are also polar in nature, and they play a significant role in numerous cellular processes, including cell crawling [6] and cell division [7]. The third type of cytoskeletal filaments are intermediate filaments, which are a broad class of fibrous crossed-linked proteins with diameter of ~ 10 nm. The presence and composition of intermediate filaments varies between cells of different tissues. Different intermediate filaments include cytoplasmic proteins, such as vimentin and keratin, and nuclear proteins, such as lamins. Like actin filaments, intermediate filaments are relatively flexible rope-like structures. Intermediate filaments do not have a primary role in cellular processes, but rather provide the cell its physical strength and serve as an anchoring scaffold for the nucleus and other organelles [8].

While rigid microtubules function as compression resisting filaments to maintain the cell's structure, the flexible intermediate and actin filaments do so by functioning as tension bearing elements. Other than providing physical support and maintaining the cell's shape and structure, the polar microtubules and actin filaments also serve as tracks for the propagation of motor proteins.

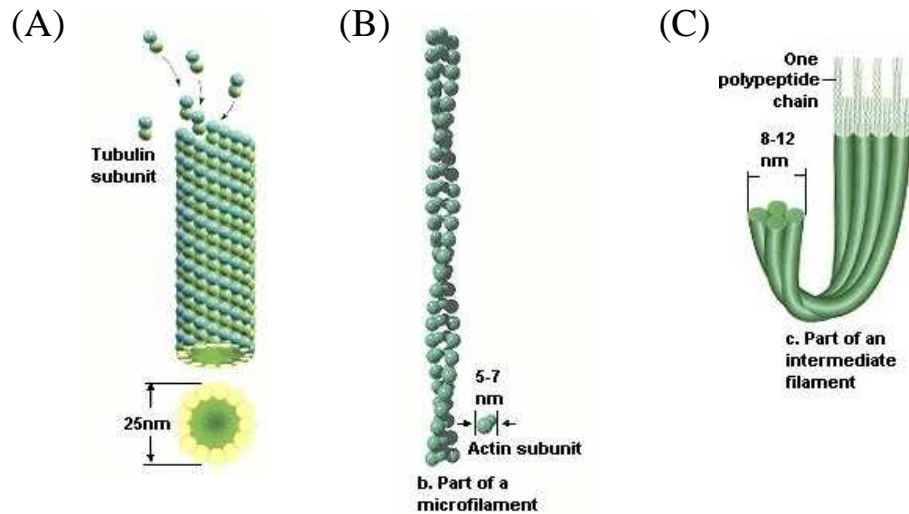


Figure 1.2: The biological cell has three main cytoskeletal filaments: (A) Microtubules are composed of tubulin dimers that form a hollow cylindrical structure with diameter ~ 25 nm. (B) Actin filaments have a double stranded structure composed of G-actin monomers. (C) Intermediate filaments are made of tetramer subunits arranged in an anti-parallel fashion, which makes intermediate filaments non-polar.

1.2 Motors proteins

Motor proteins are specialized molecules that possess the ability to convert chemical energy, derived from adenosine triphosphate (ATP) hydrolysis, into useful mechanical work [9]. The biological cell utilizes the action of these nano machines to transport vesicles, organelles and other kinds of cargo across the cell. This type of active transport is achieved by the propagation of the motors along microtubule and actin filament tracks within the cell.

Motor proteins can be divided into different classes, characterized by the filament with which they interact and the preferred direction of motion along the filament. They also vary in their degree of processivity, which is determined by the duty ratio, i.e. the fraction of time out of the entire ATP hydrolysis cycle in which a motor remains bound to the filament. For example, kinesin motors “walk” along microtubules, while myosin motors interact with actin filaments. Most kinesins and myosins move towards the plus end of the microtubules and actin filaments, respectively [27]. In contrast, Ncd motors (kinesin-related microtubule motors) and myosin VI (which propagate along actin filaments) move towards the minus

end of their associated filament tracks [11, 12]. Finally, while processive motors like kinesins can cover long distances along microtubules without detaching from the track [13], non-processive motors with a low duty ratio, like most myosin family motors, take only single steps along the actin filament before disconnection occurs [14].

One abundant non-processive motor protein is myosin II, which plays a significant role in a diversity of cellular processes. The low duty ratio of myosin II implies that these motors have a rather poor performance as individuals (unlike kinesins) and, hence, they need to work in cooperation with each other in order to produce substantial motion. The structure of myosin II consists of three major parts [see Fig. 1.3(A)]: (i) a head domain, which binds to binding sites located on the actin filament. This part is responsible for ATP hydrolysis, which triggers a conformational change that causes the motor head to rotate; (ii) a neck domain, which serves as a lever arm that amplifies the motion of the rotating head; (iii) a tail domain, which can attach cargo and organelles for transport.

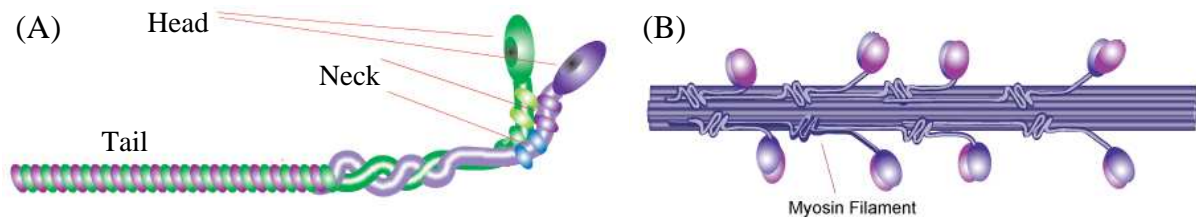


Figure 1.3: (A) Schematics of a myosin II molecule, which consists of three main regions: a head domain with an ATP hydrolysis site; a neck region that acts as a lever arm for the rotating head; a tail domain which binds cargo. (B) Myosin II molecules pack together to form thick filaments from which motor heads project. A single thick filament may consist of several hundreds of myosin II molecules.

In vertebrate striated muscles myosin II molecules pack together into bipolar myosin filaments with the tails forming a roughly cylindrical filament backbone and the myosin heads arranged in a quasi-helical array on the filament surface [see Fig. 1.3(B)].

1.3 Cooperativity between motor proteins

The collective action of motor proteins is implicated in various important cellular processes. During mitosis, for instance, interactions between kinesins motors and microtubules (which comprise the mitotic spindle) are involved in the segregation of chromosomes into two distinct part of the cell, defining the future daughter cells [15]. Moreover, in cytokinesis (the process of cell division) actin filaments arrange themselves along the cell's circumference to form the contractile ring (see Fig. 1.4). The action of myosin II motors causes the actin filaments to slide past each other, resulting in the contraction of the ring, which leads to the division of the cell into the two daughter cells [7].

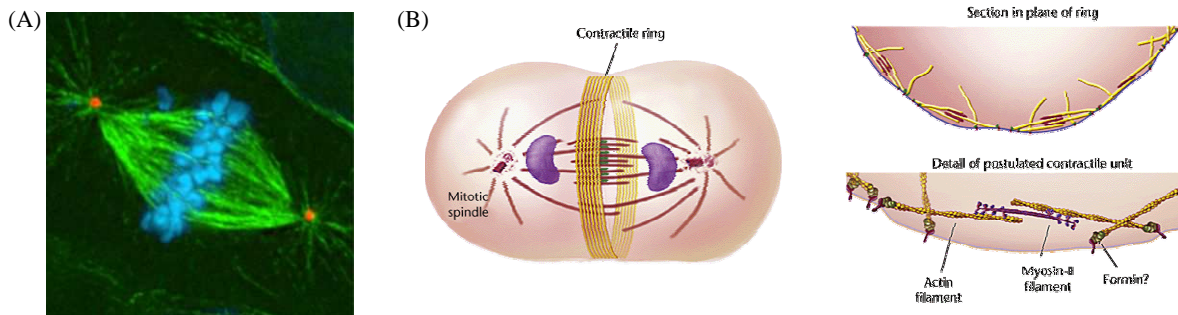


Figure 1.4: (A) A fluorescent image of the mitotic spindle showing microtubules (green), chromosomes (blue) and centrosomes (red) during the metaphase stage of cell division. (B) Following the segregation of the genetic material into opposite parts of the cell (left), the contractile ring shrinks due to the action of myosin II motors on actin filaments (right), dividing the cell into two.

Cooperative work of myosin motors is also found in the adaptation of mechanically activated transduction channels in stereocilia of hair cells in the inner ear (see Fig. 1.5). In response to an auditory stimulus, transduction channels open and generate an influx of Ca^{2+} into the stereocilia (which are composed of parallel cross-linked actin filaments). In turn, Ca^{2+} causes myosin 1-c motors to dissociate from the actin, which reduces the channel's tension and leads to its closure. When Ca^{2+} influx ceases, myosin 1-c motors climb back up the actin filaments to restore the resting tension and the native sensitivity of the hair bundle. This mechanism allows hair cells to adapt to prolonged stimuli while remaining sensitive to

new ones [16].

Cooperativity between myosin II motors can also be found in muscle contraction and *in vitro* motility assays. These two cases are further discussed below.

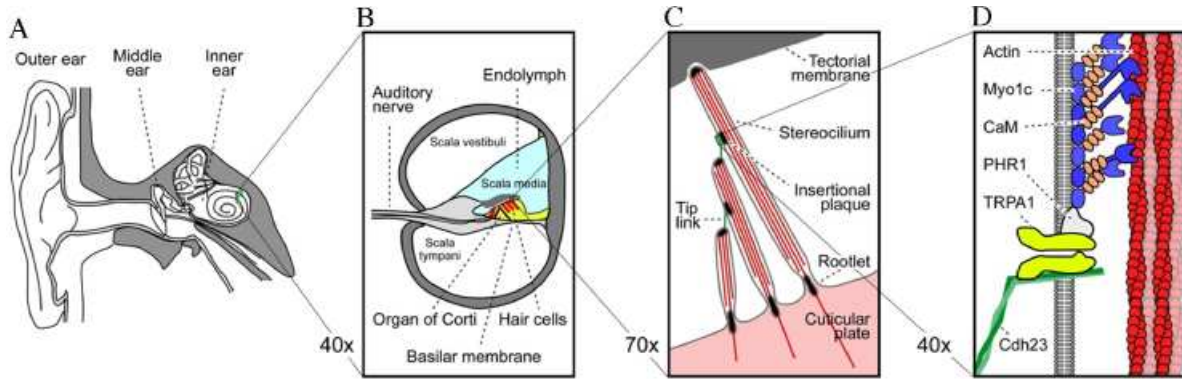


Figure 1.5: (A) The cochlea of the inner ear has a spiral structure consisting of three fluid filled chambers. (B) Cross section of the cochlea showing the hair cells that lie on top of the basilar membrane. (C) Stereocilia of hair cells arranged in rows of increasing height are deflected due to the movement of the basilar membrane, increasing tip link tension. (D) Increased tension within the tip links, connecting stereocilia, opens transduction channels. The action of myosin 1-c on actin filament restores the resting tension for new stimuli.

1.3.1 Motility assays

In vitro motility assays constitute a very useful experimental technique for studying motor dynamics in reconstituted model systems. The two main geometries used in motility assays are the bead assay and the gilding assay. In the former, the filament tracks are fixed to a coverslip, and motors are adsorbed to micro-sized beads, which are suspended in a solution with the presence of ATP. The beads first diffuse until they encounter a filament track, allowing the motors to attach to the track and propagate along it. In gliding motility assays the filaments glide over a surface covered by immobilized yet active motors (see Fig. 1.6). In both cases, either the beads (in the bead assay) or the filaments (in the gilding assay) are fluorescently labeled, and the motion is detected and analyzed by means of video microscopy. Tracking the motion of the bead or the filament provides important information, such as motor directionality, filament gliding velocities, and motor proteins

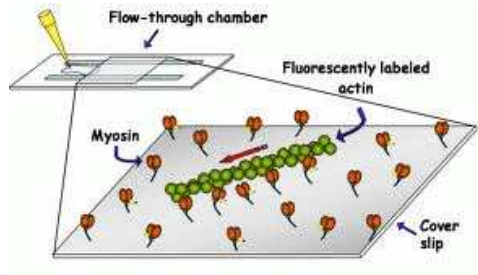


Figure 1.6: Schematic of a gliding motility assay, in which a fluorescently labeled actin filament lies on a bed of immobilized, yet active, myosin II motors. The filament's motion due to motor forces is recorded and analyzed to extract different data.

kinetic parameters. Motility assays, thus, offer an important and powerful experimental tool for understanding the nature and dynamics of motor proteins under controlled conditions.

1.3.2 Skeletal muscles

One of the more fascinating examples for the cooperative action of myosin II motors is their role in skeletal muscle contraction. Skeletal muscles are organized in a hierarchical fashion, in which the basic contractile unit is the *sarcomere*. Repeating units of sarcomeres comprise the myofibril which, in turn, lie parallel to other myofibrils to compose the multi-nucleated cylindrical muscle cell [also referred as a muscle fiber, or a myocyte (see Fig. 1.7)]. The sarcomere itself is composed of two types of filaments, actin (thin) and myosin (thick), in an arrangement that allows them to slide past each other [see Fig. 1.8(A)]. The thick filament consists of about 300 myosin II molecules, and is surrounded by 12 actin filaments, 6 around each half [see Fig. 1.8(B)]. The motors heads project out of the thick myosin filament every 14.3 nm, and the angular difference between adjacent motor heads is 40° [17]. The thin filaments in each half sarcomere lie parallel to each other, and their orientation is opposite to the thin filaments on the other half sarcomere, so that the plus ends of all thin filaments are found at the ends of the sarcomere (i.e., the Z-line). While thin actin filaments are anchored at the Z-line, thick myosin filaments are crosslinked at the M-line, which is located at the center of the sarcomere [see Fig. 1.8(A)].

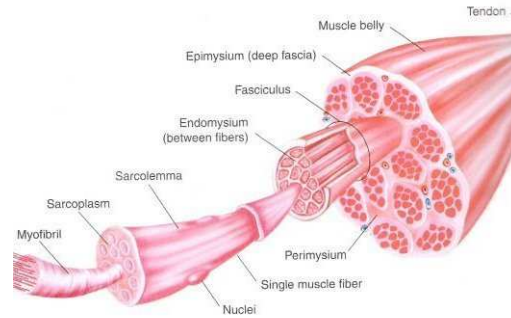


Figure 1.7: The skeletal muscle consists of bundles of fascicles made of muscle fibers, each composed of myofibrils, which are made of repeating units of sarcomeres.

When the muscle is at rest the actin filament is covered by tropomyosin, making the binding sites unavailable for the attachment of motors. Upon nervous stimulation, Ca^{2+} ions flow into the muscle cell and unlock the actin-covering tropomyosin, which results in the exposure of binding sites to the attachment of myosin II motors. Once attached to a binding site, ATP hydrolysis causes the motor head to rotate and pull the actin filament towards the M-line. The resulting sliding of thin filaments past thick filaments leads to the shortening of the sarcomere and muscle contraction.

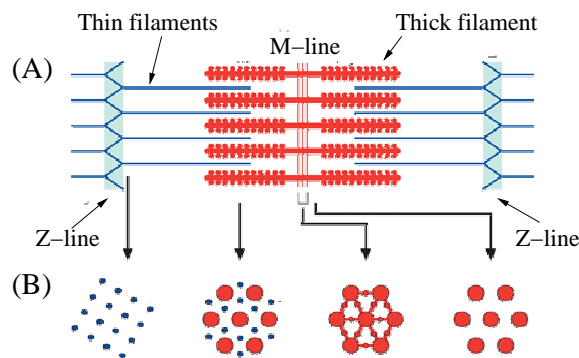


Figure 1.8: (A) The sarcomere is made of thin actin and thick myosin II filaments that slide past each other, causing the sarcomere to shorten. Actin filaments are anchored at the Z-line at both ends of the sarcomere, while myosin filaments are connected at the M-line, which is located in the center of the sarcomere. (B) Various cross-section views along the sarcomere, showing the spatial arrangement of thin and thick filaments.

1.4 Cooperative bidirectional motion

One of the more interesting outcomes of the cooperative action of molecular motors is their ability to induce bidirectional (“back and forth”) motion. This dynamical pattern emerges when filaments (or other objects such as liposomes and organelles) are subjected to the action of two groups of motors that engage in a “tug-of-war” (TOW) contest, exerting forces in opposite directions. The “victory” of the motor party that exerts the larger force determines the instantaneous direction of motion. If the two opposite forces are nearly similar, the balance of forces may shift between the two motor parties as a result of stochastic binding and unbinding events of motors to the filament track. Bidirectional motion is not restricted to cases where two classes of motors apply forces in opposite directions, but may also occur when a single group of motors interacts with a filament with mixed polarities. In a recent gliding motility, actin filaments were severed into smaller fragments and then randomly fused together to form globally a-polar actin with alternating polarities [18]. The actin filament exhibited bidirectional movement as depicted in Fig. 1.9(A). The velocity histogram of the actin shown in Fig. 1.9(B) clearly exhibits a bimodal distribution centered around zero. Fig. 1.9(C) plots a histogram of the time duration of unidirectional intervals of motion. The histogram is fitted to an exponential distribution $p(t) = (1/\tau_{\text{rev}})\exp(-t/\tau_{\text{rev}})$, from which the typical reversal time τ_{rev} between unidirectional intervals of motion was extracted. The measured reversal times were found to be macroscopically large, $\tau_{\text{rev}} \sim 3 - 10$ seconds [see Fig. 1.9(D)], which is two order of magnitude larger than the ATP-ase cycle time [9]. This observation has indicated that some cooperativity is involved in the dynamics.

One of the earlier models for cooperative bidirectional motion has been presented in 1995 by Jülicher and Prost [19] (see also later versions in [20, 21]). The model has been inspired by several ratchet models for single motor proteins [22–24], in which a motor is viewed as a particle moving in a two state system: In the attached state it experiences a periodic asymmetric potential, while in the detached state it moves freely (see Fig. 1.10). Jülicher and Prost extended this model for collective motor dynamics by connecting the motors to

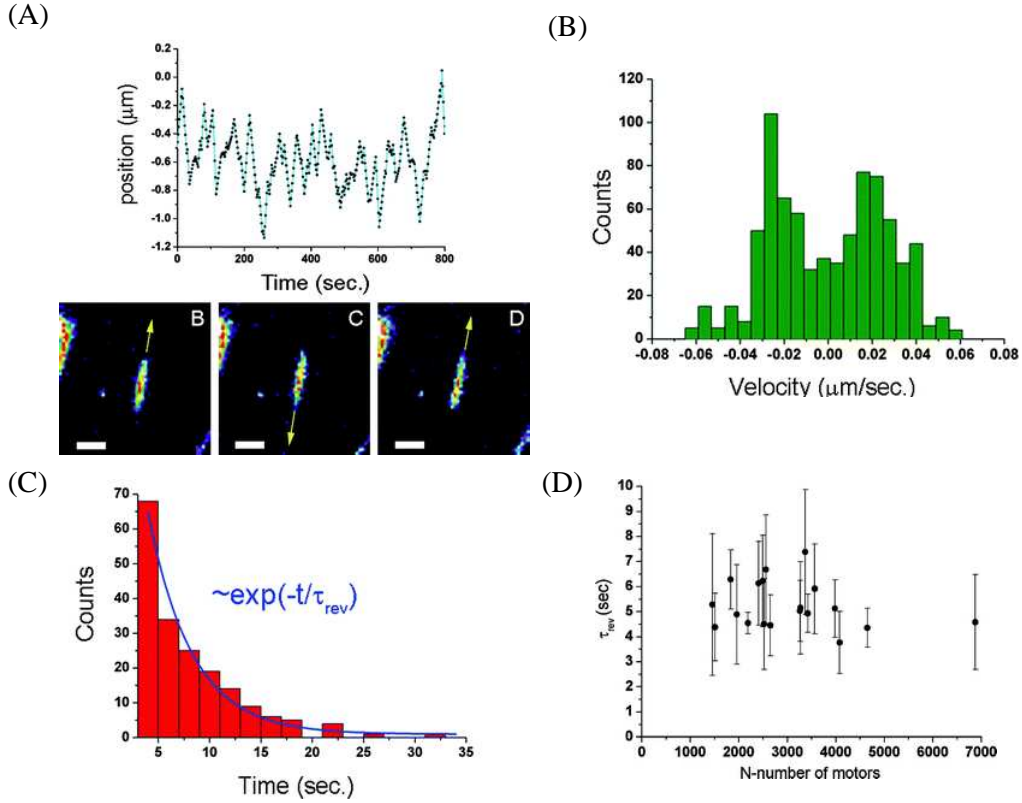


Figure 1.9: (A) The position of the a-polar actin filament with alternating polarities (top). The filament's instantaneous direction of motion (bottom). Bar size is $5 \mu\text{m}$. (B) Velocity histogram of the actin filament with alternating polarities, exhibiting a bimodal distribution centered around zero. (C) Distribution of reversal times of a single filament with alternating polarities. The distribution is fitted by a single exponential decay function with a characteristic reversal time τ_{rev} . (D) The characteristic reversal time τ_{rev} of 19 different bundles as a function of the number of motors N .

a rigid rod that enforces the particles to move together. The fact that the system is not in thermodynamic equilibrium (due to constant ATP consumption by the motors) is introduced via the assumption that the attachment and detachment rates (ω_1 and ω_2 , respectively) do not satisfy conditions of detailed balance - $w_1(x)/w_2(x) \neq \exp[-\Delta U(x)/k_B T]$. Specifically, in ref. [21] the authors assumed that

$$\frac{w_1(x)}{w_2(x)} = \exp\left(\frac{-\Delta U(x)}{k_B T}\right) + \Omega \Theta(x), \quad (1.1)$$

where the function $\Theta(x)$ and the amplitude Ω characterize the non-equilibrium (ATP-driven)

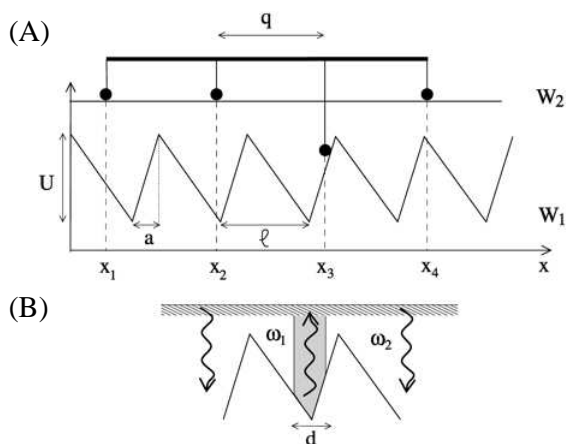


Figure 1.10: Schematics representation of the ratchet model for collective motor dynamics introduced by Jülicher and Prost. (A) The motors are connected to a rigid rod at fixed spacing q . In the attached state, the motors interact with an asymmetric potential W_1 with period l . The detached state is represented by a uniform potential W_2 . (B) The motors attachment rate w_2 (detachment rate w_1) is localized around the potential maxima (minima).

transitions. Bidirectional motion was observed when $\Theta(x)$ is defined such as that detachments occur around the minima of the potential wells, while attachments take place around the potential maxima. For $\Omega < \Omega_c$ (i.e., near thermal equilibrium) the system rapidly oscillates between left and right movement. Above a critical value Ω_c , the motion becomes bidirectional with reversal times that diverge exponentially with the number of motors N^1 . This is reminiscent of a para-ferro magnetic transition at zero external field, where below the critical temperature the up-down symmetry is spontaneously broken, with a “flip” probability that diminishes exponentially with the system size.

The experimental results reported in [18] challenged the prediction regarding the exponential growth of τ_{rev} with N . It was found that the characteristic reversal times of the bidirectional motion in this motility assay were macroscopically large, but practically independent of the number of motors [see Fig. 1.9(D)]. This observation implies that the motors interact (crosstalk) with each other - a feature that was absent in earlier theoretical studies. Crosstalk between motors may arise from direct interactions between motors that lead to correlations between their attachment states. Another possibility is that the motors

¹The critical value Ω_c depends on the form of the ratchet potential. For the asymmetric saw-tooth potential used in ref. [21] the authors found $\Omega_c \simeq 0.009\omega_2$

indirectly influence each other. This latter scenario is discussed below.

1.5 The elasticity-mediated crosstalk (EMC) effect

A recent theoretical model for bidirectional motion which incorporated the filament's compliance showed that indirect interaction between motors can be mediated by the elasticity of the actin filament. According to this model, binding and unbinding events of motors change the elastic energy stored within the elastic filament, thus altering the transition rates of motors between states. During bidirectional motion, the elastic filament is subjected to a tug-of-war between motors that exert opposite forces, which creates large stress fluctuations along the elastic filament. In order to relieve the tension within the actin and reduce these stress fluctuations, the attachment and detachment rates of the motors are modified. This type of crosstalk between motors, in which they indirectly communicate with each other through the elastic filament, has been termed the *elasticity-mediated crosstalk* (EMC) effect. Mathematically, the EMC effect can be understood by considering Eq. 1.1 and noticing that in the equilibrium term, the energy change includes two contributions,

$$\Delta U = \sum_{i=1}^N \Delta U_i^{\text{motor}} + \Delta E^{\text{el}}. \quad (1.2)$$

The first term in Eq. 1.2 is the change in the energy of the motor whose state is varied. The second term ΔE^{el} is the change in the elastic energy, occurring due to the change in the force that the motor exerts on the filament. The elasticity term is a collective term because the elastic energy depends on the states of all the motors (see section 1.5.2 below). It can be treated as an equilibrium degree of freedom since mechanical equilibrium is established on time scales that are several orders of magnitude smaller than the ATP-ase cycle.

1.5.1 System model

In order to quantify the EMC effect, we propose the following model: The actin filament is represented as a chain of N nodes connected by $N - 1$ identical elastic springs with spring constant k_s (see Fig. 1.11). In the chain's reference frame the i -th node is located at $x_i = (i - 1)\Delta l$, and, for brevity, we set $\Delta l = 1$. Each node, which represents a binding site for the myosin II motors, can be in one of two states - detached or attached. In the detached state there is no interaction between the node and a motor, and the node experiences no force. In the attached state, the motor exerts a force of magnitude f_0 on the node, in a direction that depends on the local polarity of the filament ¹.

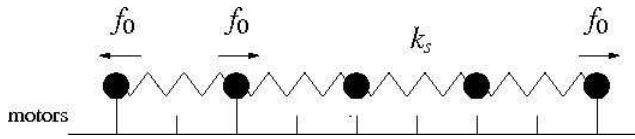


Figure 1.11: A schematics of our system model: The elastic actin track is represented by a chain of N nodes connected by identical springs with spring constant k_s . The nodes can attach to and detach from myosin II motors. An attached node experiences a force of magnitude f_0 in a directions that depends on the local polarity, while a detached one experiences no force.

The probability of a motor to be in the attached state will be denoted by r , which is the duty ratio of a single motor. It is important to note that our model uses fixed values for r and f_0 . Actually, the values of r and f_0 depend on several parameters, most importantly the instantaneous relative position of the motor head to its binding site. Our model utilizes a simplified picture, in which the temporal and spatial variations in the duty ratio between motors (which arise due to the motion of the actin filament and the incommensurability between the motors and the binding sites) are neglected. A possible way to include variations between motors is to assume that these values are chosen from certain distributions, which are centered around r and f_0 . However, for a large number of working motors N and large

¹Depending on the setup, the number of motors may be larger than the number of nodes (see, e.g., our schematic Fig. 1.11). However, each node can be attached to no more than one motor and, therefore, the excess motors (which, at a given instance, are spatially hindered from binding to one of the sites) have no impact on the chain. Thus, we will assume that the number of motors is also N , effectively ignoring the motors that cannot connect to the nodes.

times, these variations are expected to average out, thus not altering our results. This is analogous to the diffusion problem of a particle, whose step size (per unit time) is drawn from a symmetric Gaussian distribution. One can reproduce the same diffusive behavior using a different model with steps of *fixed* size that are made with equal probability in opposite directions.

Different configurations of the system are defined according to which nodes are connected to motors and which are not. The statistical weight of a configuration with n “attached” motors is given by

$$w = r^n (1 - r)^{N-n} \exp\left(-\frac{E^{\text{el}}}{k_B T}\right), \quad (1.3)$$

where T is the temperature and k_B is the Boltzmann constant. By averaging over all possible configurations, one can find the *effective* duty ratio of the i -th motor $\langle r(i) \rangle$, and the *mean* effective duty ratio $\langle r \rangle = \sum_{i=1}^N \langle r(i) \rangle / N$.

1.5.2 Calculating the elastic energy

Three types of forces are exerted on the chain’s nodes: (i) the motor forces f_i^{motor} , (ii) the spring forces F_i , and (iii) friction drag forces f_i^{drag} . Because the motion is highly overdamped, the total instantaneous force on each node vanishes. Thus, for the i -th mass the equation of motion reads

$$f_i^{\text{motor}} - f_i^{\text{drag}} + F_i - F_{i-1} = 0, \quad (1.4)$$

with $F_0 = F_N = 0$. The drag force includes two contributions - one is due to motor friction (MF), f_i^{MF} , and the other is due to friction with the surrounding viscous medium, f_i^{viscous} . The motor friction forces act only on the particles which are connected to the motors.

Therefore, by redefining the motor forces $f_i = f_i^{\text{motor}} - f_i^{\text{MF}}$, we can rewrite Eq. 1.4 as

$$f_i - f_i^{\text{viscous}} + F_i - F_{i-1} = 0, \quad (1.5)$$

where $f_i = f_0$ or $f_i = 0$ if the i -th motor is attached or detached respectively. For the chain's center of mass (CoM), the equation of motion reads

$$F^{\text{CoM}} = \sum_{i=1}^N f_i - \sum_{i=1}^N f_i^{\text{viscous}} = 0. \quad (1.6)$$

Assuming that the viscous drag force is distributed uniformly along the chain (i.e., it is equal for all nodes) and, therefore, Eq. 1.6 gives

$$f_i^{\text{viscous}} = \frac{\sum_{i=1}^N f_i}{N} = \bar{f}. \quad (1.7)$$

Using this last result, Eq. 1.5 reads

$$F_i - F_{i-1} = -f_i^*, \quad (1.8)$$

where $f_i^* = f_i - \bar{f}$ is the excess force. Since $F_0 = 0$, we find that $F_1 = -f_1^*$. Then, $F_2 = F_1 - f_2^* = -f_1^* - f_2^*$; and, in general,

$$F_i = -\sum_{j=1}^i f_j^*. \quad (1.9)$$

The elastic energy of the elastic chain, which is the sum of energies of all the springs, is given by

$$E^{\text{el}} = \sum_{i=1}^{N-1} F_i^2 / 2k_s. \quad (1.10)$$

If the motion is only partially overdamped (including in the limit of zero friction), all

the nodes move together at the same acceleration. One can repeat the above calculation and show that Eq. 1.9 remains valid.

1.5.3 The dimensionless parameter β^*

Substituting Eq. 1.10 into Eq. 1.3 yields

$$w = r^n (1 - r)^{N-n} \exp \left(-\beta^* \sum_{i=1}^{N-1} \tilde{F}_i^2 \right), \quad (1.11)$$

where \tilde{F}_i is the reduced force exerted on the i -th spring (in units of f_0), and the dimensionless parameter

$$\beta^* = \frac{f_0^2}{2k_s k_B T} \quad (1.12)$$

is the ratio between the typical elastic energy of a spring $f_0^2/2k_s$ and the thermal energy $k_B T$. Eq. 1.12 relates the dimensionless parameter β^* to three physical parameters of the system: the temperature T , the typical force exerted by a motor f_0 , and the effective spring constant of the actin filament segment between two binding sites of the motors, k_s . The latter parameter can be further expressed as

$$k_s = \frac{YA}{l}, \quad (1.13)$$

where Y is Young's modulus of the actin, A is the cross-sectional area of an actin filament and l is the distance between binding sites. For myosin II motors, forces in the range of $f_0 = 5 - 10$ pN have been measured experimentally [25, 26]. The actin-cross sectional area (including the tropomyosin wrapped around the actin helix) is $A = 23 \text{ nm}^2$, and the Young's modulus of the actin-tropomyosin filament is $Y = 2.8 \text{ GPa}$ [27, 28].

The value of l is somewhat more difficult to assess. One possibility is that $l \simeq 5.5 \text{ nm}$, which is simply the size of the G-actin monomers, each of which includes one binding site

for myosin motors [29]. Another possible value is related to the double helical structure of F-actin and the fact that it completes half a wist about every 7 monomers, i.e. every $\simeq 38.5$ nm [30]. Since the binding sites follow a twisted spatial path along the double helix, many of them remain spatially unavailable to the motors in motility assays, where the motors are located underneath the F-actin. Thus, in gliding motility assays the distance between the binding sites along the line of contact with the bed of motors is $l \simeq 38.5$ nm. Two other choices for l , which are more relevant to skeletal muscles, arise from the spatial arrangement of thin and thick filaments in the sarcomere, where an average of three thick myosin filaments surround each thin actin filament. Along the thick filament, the separation between collinear motor heads is $\simeq 43$ nm [31–33]. On the other hand, the half pitch of the thin actin filament is $\simeq 38.5$ nm. The last two structural attributes of thick and thin filaments lead to two other possible values for the effective distance between nodes - $l = 43/3 \simeq 14.3$ nm ,and $l = 38.5/3 \simeq 12.6$ nm. Using the above mentioned values of the system parameters, we find that β^* lies within the range of $2.5 \times 10^{-4} \lesssim \beta^* \lesssim 7 \times 10^{-3}$.

1.5.4 Stress fluctuations

According to Eq. 1.10, the elastic energy of a given spring i is directly related to the sum of excess forces actin on all the nodes located on one side of the specific spring. Generally speaking, the elastic energy of the springs becomes larger when the force fluctuations are larger. In the motility assay described in ref. [18], featuring actin filaments with alternating polarities, the motors exert forces in opposite directions along the filament, which implies that the force fluctuations can be quite large [see Fig. 1.12(B)]. This is not the case in conventional motility assays, where the forces act in the same directions, leading to smaller force fluctuations [see Fig. 1.12(A)] . Using a scaling argument based on the statistics of random walks, the authors of ref. [18] show that the elastic energy of a bipolar actin track

with N nodes and n attached motors scales as ¹

$$\frac{E^{\text{el}}}{k_B T} \propto Nn. \quad (1.14)$$

Thus, the detachment of a single motor ($n \rightarrow n - 1$) leads, on average, to an energy gain of

$$\frac{\Delta E^{\text{el}}}{k_B T} = -\alpha N, \quad (1.15)$$

where α is some dimensionless parameter (that is closely related to the dimensionless parameter β^* described above). Eq. 1.15 implies that if N is large, the elastic energy released due to the detachment of even a single motor can be large, which is the reason why the EMC effect is significant in tug-of-war situations. The authors of ref. [18] have incorporated the EMC effect into their model by introducing an additional detachment rate that depends on the elastic energy: $w_3 = w_3^0 \exp(-\Delta E^{\text{el}}/k_B T) = w_3^0 \exp(-\alpha N)$. This additional detachment rate eliminates the exponential dependence of the bidirectional motion reversal time, τ_{rev} , on the system size N , which was predicted by earlier theoretical studies.

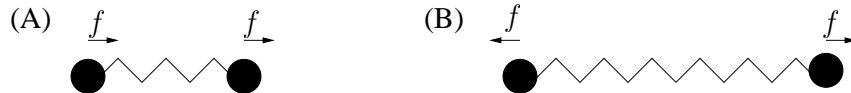


Figure 1.12: (A) In a conventional motility assays, the motors exert forces in the same direction and the springs are barely stretched. (B) In contrast, when the motors exert forces in opposite directions, the springs are more stretched, and have a much larger elastic energy.

1.6 Outline

In bidirectional motion, the origin of the EMC effect are large stress fluctuations along the actin filament due to opposite motor forces. Overall, the EMC effect reduces the attachment probabilities of motor, making each motor effectively less processive. In chapter 2 of this

¹In chapter 2 we show that, in contrast, in a conventional motility assay with polar filaments the elastic energy scales only as $E^{\text{el}}/k_B T \propto \sqrt{Nn}$.

thesis we investigate the role of the EMC in the more common case of gliding motility assays, where polar actin filaments move directionally under the action of unidirectional forces. We present a statistical-mechanical analysis and derive an analytical expression for the effective duty ratio of myosin II motors in gliding motility assays. We also conduct Monte Carlo (MC) computer simulations to verify our model. We show that, in contrast to the case of bidirectional motion (where the attachment probability is greatly influenced by the EMC effect), in gliding motility assays the EMC effect has a much weaker impact, and the effective attachment probability of myosin II motors, $\langle r \rangle$, is only slightly smaller than their duty ratio, r .

In chapter 3 we investigate the role of the EMC effect in muscle contraction. We first present a simple derivation of Hill's equation for muscle contraction, based on Newton's first law and the experimental data in ref. [34]. We conduct MC simulation to show that the EMC effect leads to a non-uniform attachment probability along the actin filament. We argue that while these non-uniformities may impair myosin II to cooperate efficiently, this effect becomes significant only when the size of the system exceeds that of the sarcomere in skeletal muscles. This observation may serve as an explanation for the remarkable similarities in the size of sarcomeres across different vertebrate species. In chapter 4 we summarize our research and discuss future possible extensions.

Chapter 2

The EMC effect in gilding motility assays

For the actin filament with alternating polarities, the EMC is a cooperative effect that reduces the degree of cooperativity between motors by decreasing their duty ratio (i.e., their attachment probability). As discussed above, much of the strength of this effect is related to the large stress fluctuations that develop in the elastic filament due to the opposite forces applied by the antagonistic motors. Conversely, in conventional motility assays a single group of motors exert forces in the same direction, leading to much smaller stress fluctuations along the elastic actin track. Thus, one can expect the EMC effect to have only a minor impact on the effective attachment probability of the motors. In this chapter we investigate the importance of the EMC effect in conventional motility assays. In section 2.1 we calculate the effective (mean) attachment probability of the motors, $\langle r \rangle$, as a function of the “bare” attachment probability r and the dimensionless parameter β^* (see section 1.5). Our analytical predictions are compared to Monte Carlo simulations in section 2.2. In section 2.3 we discuss the model parameter values characteristic for actomyosin motility assays. Specifically, we show that $\beta^* \ll 1$, which implies that the EMC effect indeed plays only a minor role in such systems. We summarize and discuss our results in section 2.4.

2.1 Statistical-mechanical analysis

To analyze the role of the EMC effect in conventional gliding motility assays, we use the model depicted in section 1.5.1. To properly examine the case of motility assays, we assume that the chain of nodes represents a polar filament ,i.e., all the motors exert forces in the same direction. As it is more convenient to analyze this problem using continuous function, we introduce the function $h(x)$ which, for $x_i < x < x_{i+1}$, has slope +1 if the monomer at x_i is connected to a motor, and a slope 0, otherwise. Thus, $h(x)$ gives the total force applied on the chain up to the point x (in units of f_0), with $h(x = 0) = 0$ and $h(x = N) = n$, where n is the number of nodes connected to motors in a given configuration. The solid line in Fig. 2.1 shows the function $h(x)$ corresponding to the attachment configuration of five nodes depicted in Fig. 1.11. To calculate the elastic energy of a configuration, we introduce the function $g(x) = h(x) - (n/N)x$, which is depicted by the dashes line in Fig. 2.1 and gives the total *excess* force accumulated up to x (in units of f_0). From Eq. 1.10 we find that the

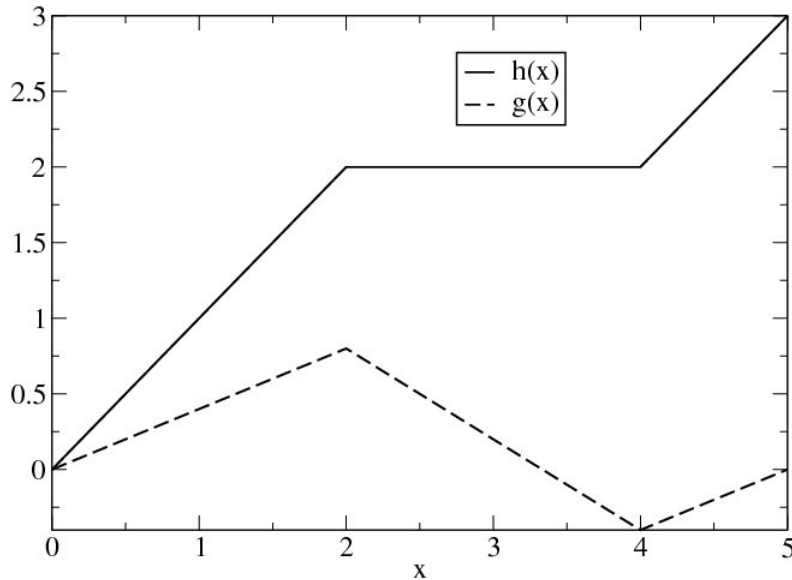


Figure 2.1: The function $h(x)$ and $g(x)$ which correspond to the attachment configuration depicted in Fig. 1.11, with all attached motors exerting forces in the same direction.

elastic energy can then be expressed as:

$$\frac{E_j^{el}}{k_b T} = \beta^* \sum_{i=1}^N g^2(x_i) \simeq \beta^* \int_0^N g^2(x) dx, \quad (2.1)$$

To determine the mean number of connected motors, one needs to calculate the partition function

$$Z = \sum_{n=0}^N r^n (1-r)^{N-n} z_n, \quad (2.2)$$

where r is the “bare” attachment probability of a single motor (i.e., its duty ratio) and z_n is the partition function of all the configurations with exactly n connected motors. The function z_n can be calculated by tracing over all the functions $g(x)$ corresponding to configurations with n connected motors. Mathematically, the condition that exactly n motors are connected can be expressed through the following constraint on the function $h(x)$.

$$\lim_{\alpha \rightarrow \infty} \int_0^N \left| \frac{dh}{dx} \right|^\alpha dx = n. \quad (2.3)$$

To allow an analytical solution, we approximate this constraint by setting $\alpha = 2$, in which case Eq. 2.3 can be expressed in terms of $g(x) = h(x) - (n/N)x$ as

$$\int_0^N \left(\frac{dg}{dx} \right)^2 dx = N \frac{n}{N} \left(1 - \frac{n}{N} \right) \quad (2.4)$$

With Eq. 2.4, the partition function z_n is given by

$$z_n = B(n, N) \int \mathcal{D}[g(x)] \exp \left(-\beta^* \int_0^N g^2(x) dx \right) \delta \left[\int_0^N \left(\frac{dg}{dx} \right)^2 dx - N \frac{n}{N} \left(1 - \frac{n}{N} \right) \right] \quad (2.5)$$

where δ is Dirac’s delta-function, and $\mathcal{D}[g(x)]$ denotes a trace over all possible realizations of the function $g(x)$. The function $B(n, N)$ is introduced in Eq. 2.5 in order to compensate for the error introduced by the approximated constraint Eq. 2.4. We will determine this

function through the requirement that for $\beta^* = 0$, i.e. in the absence of elastic crosstalk between the motors,

$$z_n|_{\beta^*=0} = \binom{N}{n} = \frac{N!}{n!(N-n)!}, \quad (2.6)$$

which is simply the number of ways to choose n out of N monomers.

In order to calculate the partition function z_n , we use the Fourier space representation of $\delta(x)$,

$$\delta(x-a) = \frac{1}{2\pi i} \int_{-i\infty}^{i\infty} e^{w(x-a)} dw, \quad (2.7)$$

and the Fourier series of $g(x)$,

$$g(x) = \sum_{k=-N/2}^{N/2-1} g_k e^{i\frac{2\pi}{N}kx}. \quad (2.8)$$

Substituting Eqs. 2.7 and 2.8 into eq. 2.5 yields:

$$z_n = B(n, N) \frac{1}{2\pi i} \int_{-i\infty}^{i\infty} dw \int \mathcal{D}[g_k] \exp \left[wN \frac{n}{N} \left(1 - \frac{n}{N} \right) \right] \times \exp \left[- \sum_k g_k^2 \left(\frac{8\pi^2}{N} k^2 w + 2N\beta^* \right) \right]. \quad (2.9)$$

Tracing over g_k can be readily performed, giving

$$z_n = B(n, N) \frac{1}{2\pi i} \int_{-i\infty}^{i\infty} dw \exp \left[wN \frac{n}{N} \left(1 - \frac{n}{N} \right) \right] \left\{ \prod_{k=0}^{N/2} \frac{\pi}{2N\beta^* + 8\pi^2 k^2 w / N} \right\}. \quad (2.10)$$

The integral over w can be evaluated using the method of steepest descent, which yields:

$$z_n \simeq B(n, N) e^{G(w_0)}, \quad (2.11)$$

where,

$$\begin{aligned}
G(w) &= n \left(1 - \frac{n}{N}\right) w - \sum_{k=0}^{N/2} \ln \left[\frac{1}{\pi} \left(\frac{8\pi^2}{N} k^2 w + 2N\beta^* \right) \right] \\
&\simeq N \left\{ w \frac{n}{N} \left(1 - \frac{n}{N}\right) - \frac{1}{2} \ln \left[\frac{2e^{-2N}}{\pi} (\pi^2 w + \beta^*) \right] - \sqrt{\frac{\beta^*}{\pi^2 w}} \tan^{-1} \left(\sqrt{\frac{\pi^2 w}{\beta^*}} \right) \right\},
\end{aligned} \tag{2.12}$$

and w_0 satisfying

$$\left. \frac{dG}{dw} \right|_{w_0} = \frac{n}{N} \left(1 - \frac{n}{N}\right) - \frac{1}{2w_0} + \frac{1}{2} \sqrt{\frac{\beta^*}{\pi^2 w_0^3}} \tan^{-1} \left(\sqrt{\frac{\pi^2 w_0}{\beta^*}} \right) = 0. \tag{2.13}$$

For $\beta^* \ll 1$, one gets

$$w_0 \simeq \frac{N}{2n} \left(\frac{N}{N-n} \right) - \sqrt{\frac{N}{8n} \left(\frac{N}{N-n} \right) \beta^*}. \tag{2.14}$$

From Eqs. 2.6, 2.11, 2.12, and 2.14, one finds that

$$B(n, N) = \binom{N}{n} e^{-G(w_0)} = \binom{N}{n} \left(\frac{\pi}{e^3} \right)^{(N/2)} \left(\frac{N^3}{n(N-n)} \right)^{N/2}. \tag{2.15}$$

Inserting Eq. 2.14 into Eq. 2.12, and expanding $G(w_0)$ in powers of $\sqrt{\beta^*}$, yields

$$G(w_0) \simeq G(w_0)|_{\beta^*=0} - \sqrt{\frac{n(N-n)}{2}} \beta^*. \tag{2.16}$$

Finally, for $\beta^* \ll 1$, the partition function z_n is obtained by substituting Eqs. 2.15 and 2.16 into Eq. 2.11, which gives:

$$z_n \simeq \binom{N}{n} \exp \left(-\sqrt{\frac{n(N-n)}{2}} \beta^* \right). \tag{2.17}$$

In order to calculate the partition function Z , one needs to substitute Eq. 2.17 into

Eq. 2.2, which gives:

$$Z = \sum_{n=0}^N \binom{N}{n} r^n (1-r)^{N-n} \exp\left(-\sqrt{\frac{n(N-n)}{2}} \beta^*\right). \quad (2.18)$$

In the thermodynamic limit ($N \gg 1$), the sum in Eq. 2.18 is dominated by one term which corresponds to the mean number of attached motors $\langle n \rangle$. This term is given by

$$\langle n \rangle = N \left[r - (1-2r) \sqrt{\frac{r(1-r)}{8}} \beta^* \right]. \quad (2.19)$$

From Eq. 2.19 we identify the *effective* attachment probability as

$$\langle r \rangle \equiv \frac{\langle n \rangle}{N} = r - (1-2r) \sqrt{\frac{r(1-r)}{8}} \beta^*. \quad (2.20)$$

Notice that the second term on the right hand side of Eq. 2.20 is anti-symmetric around $r = 1/2$, and that for $r < 1/2$ ($r > 1/2$), the effective attachment probability $\langle r \rangle$ is smaller (larger) than r . This observation is directly related to the fact the elasticity-mediated crosstalk effect is driven by the tendency to reduce the force fluctuations along the elastic filament. For $r < 1/2$ ($r > 1/2$) the force fluctuations are reduced by the detachment (attachment) of motors, which brings the system closer to the limiting case $r = 0$ ($r = 1$) where the force fluctuations vanish.

2.2 Gliding assay computer simulations

To test the validity and range of applicability of Eq. 2.20, we conducted Monte Carlo (MC) simulations of elastic chains of $N = 1000$ monomers with $r = 0.05$, which is the typical duty ratio of myosin II motors [26]. Systems corresponding to different values of β^* were simulated using the parallel tempering method. The simulations include two types of elementary moves (which are attempted with equal probability) - one in which the state (con-

nected/disconnected) of a randomly chosen node changes, and the other in which two randomly chosen nodes with opposite states change their states simultaneously. For each move attempt, the model energy of the chain E^{el} is recalculated, and the move is accepted/rejected according to the conventional Metropolis criterion with the statistical weights given by Eq. 1.3. As discussed in section 1.5, we treat the elastic energy of the actin E^{el} as an equilibrium degree of freedom since the mechanical response of the filament to changes in the attachment states of motors is extremely rapid and occurs on time scales which are far shorter than the typical attachment time of motors. The assumption that the actin filament is at mechanical equilibrium is also made in theoretical studies of intracellular cargo transport [35] and muscle contraction [36].

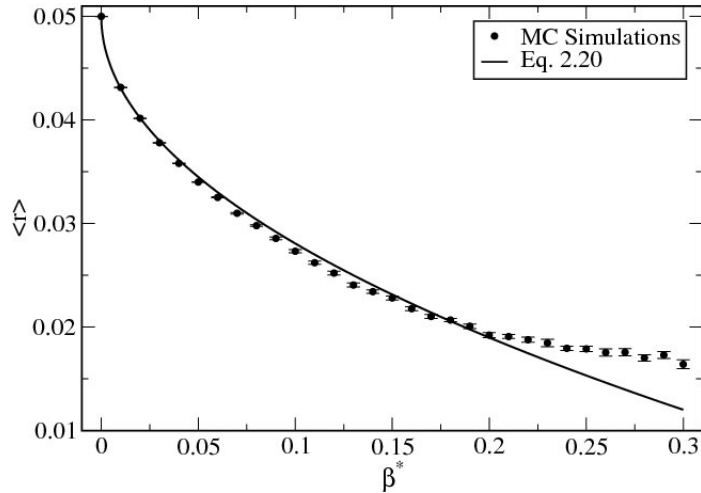


Figure 2.2: The effective attachment probability as a function of the dimensionless parameter β^* . The circles denote the results of the MC simulations, while the solid line depicts the analytical approximation for $\beta^* \ll 1$, Eq. 2.20.

Our MC results are summarized in Fig. 2.2. For $\beta^* < 0.2$, we find an excellent agreement between our computational results and Eq. 2.20 (which has been derived for $\beta^* \ll 1$). Notice that Eq. 2.20 does not include *any* fitting parameters. For larger values of β^* , Eq. 2.20 overestimates the decrease in $\langle r \rangle$.

2.3 Actin-Myosin II systems

For the duty ratio r , the range of experimental values is scattered and varies from $r = 0.01 - 0.02$ [9] to $r = 0.05$ [26]. The uncertainty may be partially related to the EMC effect discussed here. It also stems from the fact that r also depends on the distance and orientation of the motor head (both in space and time) with respect to the associated binding site. These may vary between the motors which, hence, should have different attachment probabilities ¹. Setting the duty ratio of myosin II to $r = 0.05$ (as used in the MC simulations) we find that for the range of β^* estimated in section 1.5.3, the *effective* duty ratio is slightly lower than r and lies within the range of $\langle r \rangle = 0.97r$ (for $\beta^* = 2.5 \times 10^{-4}$) and $\langle r \rangle = 0.88r$ (for $\beta^* = 7 \times 10^{-3}$). Using a lower estimate for the duty ratio $r = 0.02$ [9], we find that the effective duty ratio drops to $0.80r \lesssim \langle r \rangle \lesssim 0.96r$ for the same range of β^* .

As stated earlier, the cooperative action of myosin motors “compensates” for the non-processive character of the individual motors. The mean force generated by a group of N motors is $\langle F \rangle = N \langle r \rangle f_0$. Which force f_0 maximizes the effective force per motor $f_{\text{eff}} = \langle F \rangle / N$ and, hence, the force production of the collectively working motors? From Eq. 1.12 and 2.20 we find that the maximum value of f_{eff} is achieved when the force of the individual motors is

$$f_0^{\text{max}} = \frac{2r}{1 - 2r} \sqrt{\frac{k_s k_B T}{r(1 - r)}} \quad (2.21)$$

Setting the values of the system parameters as above ($Y = 2.8$ GPa, $A = 23$ nm², $l = 38$ nm) and taking $r = 0.02$ as the duty ratio of a single motor, we find that $f_0^{\text{max}} \simeq 25$ pN, for which $f_{\text{eff}} \simeq 0.25$ pN. For forces in the range of $f_0 \simeq 5 - 10$ pN, which are typically measured for myosin II motors [26], the effective mean force per motor is $f_{\text{eff}} \simeq 0.1 - 0.15$ pN, which is about half of the optimal effective force $f_{\text{eff}}(f_0^{\text{max}})$. We, thus, conclude that myosin II

¹In our statistical-mechanical analysis, r represents the typical duty ratio of individual myosin II motors, which are all assumed to have the same r . It is possible that accounting for the variations in r in the model will result in a slight increase in the magnitude of the elasticity crosstalk effect.

motors work quite close to conditions that maximize their cooperative force generation.

2.4 Summary

The growing interest in the collective behavior of molecular motors have led to numerous theoretical studies over the past years, especially in relation to cooperative dynamics of cytoskeletal filaments in motility assays. Most of these studies have focused on the bidirectional motion arising when the filament is driven by two groups of antagonistic motors, or when a single motor party works against an external force. The findings of ref. [18] have demonstrated that the duty ratio of motors (and, hence, the degree of cooperativity between them) is effectively reduced by the elasticity of the actin filament.

In this chapter we have extended our studies and analyzed the role of the EMC effect in gliding motility assays, where similar motors act on a polar filament in the absence of a counter external force. We used a statistical-mechanical calculation to derive an analytical expression for the effective attachment probability $\langle r \rangle$. from the partition function associated with the filament elastic energy. The analysis shows that due to the EMC effect, $\langle r \rangle$ takes a slightly smaller value than the “bare” attachment probability of a motor r . This result is quite different from the previous findings for motility assays of bidirectional motion, where the EMC effect has a much greater impact. Within the range of small values of β^* (which is the case for myosin II motors), the presented model is in a very good agreement with the results from our computer simulations.

In order to single out the EMC effect from other possible collective effects (e.g. those associated with non-equilibrium ATP-assisted processes and the elasticity of the motors themselves [37–39]), we neglect motor to motor variations and use a model in which the motors are characterized by two mean quantities: the bare attachment probability to a non-elastic rigid filament r , and the mean applied force f_0 (see discussion in section 1.5.1). This mean field description is expected to hold when the number of motors N becomes large.

However, the characterized mean duty ratio of a motor r and the motor force f_0 actually do depend on the filament sliding velocity v . In the next chapter we discuss how this notion is related to the EMC effect and what does it imply on the effective attachment probability of motors $\langle r \rangle$, when the filament is subjected to an external force, as in the case of muscle contraction.

Chapter 3

The EMC effect in muscle contraction

Skeletal muscle contractility is governed by interactions between thick myosin II filaments and thin actin filament tracks. Over the past century, several important theoretical studies have emerged in the attempt to better understand the underlying mechanisms of myosin II cooperative work in skeletal muscle. Similar to the case of bidirectional motion where antagonistic motor parties exert forces in opposite directions on the elastic actin filament, muscle contraction also displays a tug-of-war contest between a single group of motors and an external force. What effect does the EMC has in this kind of a setup, and what are the consequences regarding muscle contraction? The following chapter aims to address these questions. In section 3.1 we review the key developments in our current understanding of muscle contractility, starting from the early work of Hill and his phenomenological equation for the load-velocity relationship of muscles, and reaching to modern mechano-chemical models. In section 3.2 we return to Hill's equation and rederive it in light of some new experimental findings (which we will investigate in our review section 3.1). Finally, we will investigate the relevance of the EMC to the problem of muscle contraction in sections 3.3 and 3.4. Our results are summarized and discussed in section 3.5.

3.1 Muscle contraction models

Comparison of skeletal muscle cells in different vertebrates reveals that the lengths of their sarcomeres are almost identical. More specifically, the length of the thick filament is usually found to be close to $1.6 \mu\text{m}$, while the length of the thin filament is typically in the $0.95 - 1.25 \mu\text{m}$ range [40]. The fact that the dimensions of the sarcomere have been preserved through the course of evolution is remarkable, considering the different tasks that different muscles perform in different species. As discussed in section 1.3.2, coordinated action of motors is ubiquitous for muscle contractility (as well as other processes described above) due to the low processivity of myosin II.

The structure of the acto-myosin sarcomere was fully resolved by the late 60s' [41]; but our current understanding of the mechanics of muscle contraction is actually very much influenced by two earlier classical works. The first one is A. V. Hill's work (1938) [42], in which the muscle was represented through a combination of elastic, contractile, and resistive (viscous) elements. Hill postulated that in overcoming the viscous resistance, the contracting muscle does work and produces heat. Through a general notion of energy balance and some empirical relations between the rate of heat production during muscle contraction and the contraction velocity, Hill derived his famous equation:

$$(P + a)(v + b) = (P_0 + a)b, \tag{3.1}$$

where P is the load opposing the contraction, v is the contraction velocity, P_0 is the isometric load (i.e., the load for $v = 0$) and a and b are constants. Eq. 3.1 describes a hyperbolic relation between P and v . Although generally considered as a phenomenological force-velocity relationship rather than a thermo-mechanical expression, Hill's equation has drawn much attention because of its simplicity and the agreement it shows with experimental measurements [43].

The second milestone paper was published in 1957 by Huxley, where he laid out his

crossbridge theory [44]. The crossbridge model provides a molecular-level interpretation for muscle contraction. Within the model, the myosin motor heads interact with specific binding sites along the actin filament to form elastic crossbridges. When a motor is attached to a binding site, the crossbridge stretches and force is applied on the actin filament, resulting in the relative movement of the actin (thin) and myosin (thick) filaments past each other. The attachment and detachment of motor heads to and from the actin filament are governed by “on” and “off” rate functions that regulate the fraction of crossbridges (i.e., attached motors), and which depend on the stretching energy of the crossbridges. The “on” and “off” rates were chosen by Huxley to obtain a good fit with Hill’s experimental data for the force-velocity ($P - v$) relationship (Eq. 3.1).

Huxley’s work, together with the development of improved methods for experimental determination of the sarcomere’s micro-structure [45], as well as new biochemical measurements of ATP activity [46], have provided a fruitful field for further investigations. A large body of work has been devoted to expanding Huxley’s two-state model into more sophisticated schemes that describe more adequately the working cycle of the myosin motors. The most important chemical states comprising the mechanochemical cycle of myosin II are described by Lymn-Taylor four-state scheme [47]. According to this scheme, which is schematically depicted in Fig. 3.1, a myosin motor captures an ATP molecule and hydrolyzes it into a phosphate unit (Pi) and ADP. It then binds to a proximal binding site of the actin. Release of the Pi triggers a conformational change during which the motor head rotates. This stage is known as the “power stroke” that propels the myosin II motor along the actin filament. At the end of the power stroke, ADP is released, ATP rebinds to the myosin motor that rapidly dissociates from the actin, ready to repeat the cycle. One of the first models that integrated the Lymn-Taylor scheme into Huxley’s crossbridge theory was introduced by Duke [36]. Duke’s *stochastic-elastic* model (which inspired several other works) is based on two key principles which already existed in Huxley’s theory. The first one is the assumption that the motor heads are elastic elements whose chemical on and off rates are

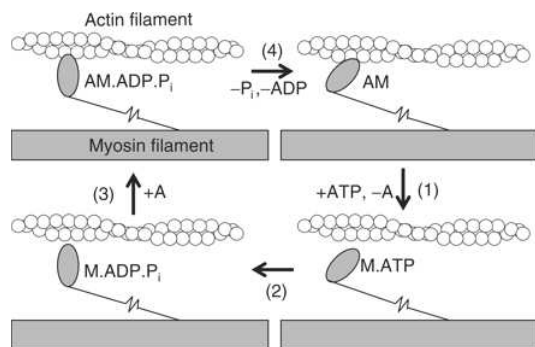


Figure 3.1: The Lymn-Taylor model for the cross bridge cycle. (1) The motor head binds ATP and dissociates from the actin. (2) ATP is hydrolyzed into ADP and Pi. (3) The motor head binds to the actin. (4) Release of the hydrolysis products causes the motor head to rotate and pull the actin filament. At the end of the cycle myosin rebinds ATP and the cycle is ready to repeat.

strain-dependent. The second key assumption is to neglect the viscous friction force in the equation of motion of the contracting muscle. The last assumption can be justified by a simple fluid-mechanics calculation for the motion of a thin rod in a medium with viscosity similar to water [48]. One can easily check that the friction force on a thin rod (with diameter $\simeq 5.5$ nm and length $\simeq 1.1$ μm) is in the fN-range, which is 3-4 order of magnitude smaller than the typical motor forces which are in the pN-range [26]. The last assumption implies that when the muscle contracts *at constant velocity*, the sum of motor forces exactly balances the external force opposing the contraction. To solve his stochastic model and obtain the force-velocity relationship, Duke used kinetic Monte Carlo (MC) simulations [49,50] in which: (i) the elastic energy and the associated reaction rates are calculated for each motor, (ii) the state of one randomly chosen (with probability proportional to the corresponding reaction rate) motor is changed, which disrupts the balance of forces in the system, and (iii) the actin filament is advanced to a new position where mechanical equilibrium is reestablished.

Following Duke's work, several stochastic-elastic models with increased level of complexity were published [51–56], which succeeded in reproducing Hill's force-velocity relationship. Another major success of this class of models is their ability to show that the fraction of working (force-producing) motors, r , increases with the load P . This interesting feature

of skeletal muscles has been recently observed by Lombardi and co-workers [34]. Using X-ray scattering and mechanical measurements on tibialis anterior muscles of frogs, they showed that r increases from roughly $r = 0.05$ for $P = 0$ (which is comparable to the duty ratio measured for myosin II motors in motility gliding assays [57]) to $r = 0.3$ for the maximal isometric load. However, despite the successes of the stochastic-elastic models, controversy remains concerning the purely elastic nature of these models. How can the sarcomere function as a low Reynolds number system with constant velocity in the absence of significant friction forces? To restate this puzzle, consider the aforementioned kinetic MC simulations of the stochastic-elastic model, where a change in the state of one motor takes the actin filament out of mechanical equilibrium and causes it to move. But if friction forces can be neglected in favor of the motor forces, why should the actin filament stop at the new position of mechanical equilibrium and not continue past this point with inertia? Obviously, one may argue that the motion is erratic only on the microscopic time scales of the motor cycle, but appears smooth on the larger time scales corresponding to sarcomere shortening. However, this explanation is somewhat unsatisfactory considering the fact that the elastic-stochastic models are based on detailed descriptions of the transitions between different mechanochemical states of the motors. Thus, it is not surprising that alternative theories incorporating viscous effects have been also proposed for the contractile process. One of the first such theories is the “impulsive model” of Worthington [58] which, in stark contrast to Huxley’s view, assumes that the motors operate by exerting impulsive forces on the actin. According to this theoretical approach, the viscous force for active muscles is comparable to the motor forces, i.e. 3-4 orders of magnitude larger than Huxley’s hydrodynamic estimate [59]. Presumably, the relevant viscosity is that of the cytoplasmatic environment, which is indeed much larger than the viscosity of water [60,61]. More recently, Landesberg *et al.* introduced a four-state model in which the motors are represented as viscoelastic, rather than purely elastic, elements [62]. The transition rates between the different states of the viscoelastic motors depend on the sliding velocity (strain rate) and not on the displacement (strain) of

the motor heads. This model has been capable of reproducing many features of muscles, including the derivation of Hill’s equation, as well as the increase in the number of working motors with the load. The model neglects the viscous friction with the embedding medium (which is taken to be water), and proposes that the friction originates from the crossbridges themselves. Accordingly, the force applied on the filament by the motors decrease linearly with the sliding velocity v , and vanishes in the absence of an external load. Nevertheless, this feature of the model is not supported by Lombardi’s finding that the force per motor depends only weakly on v (see Fig. 4(B) in ref. [34]).

The increase in the fraction of attached motors with the load can be considered as a reflection of motor cooperativity. A careful inspection of the different existing models reveals that the origin of this effect is the increase in the duration of the power stroke step of the motor cycle with P or, in other words, the increase in the detachment rate of the motors with v . As discussed in section 1.4, related patterns of collective behavior also emerge in physical ratchet models for motor protein motility assays [20,21]. Specifically, several ratchet models have shown that when motors are engaged in “tug-of-war” competitions, their detachment rates may be considerably varied [35,63].

One of the factors that significantly contributes to the changes in the detachment rates during tug-of-war is the EMC effect [31]. The opposite forces engaged in a tug-of-war contest can be applied by two groups of antagonistic motors (as in the motility assay described in ref. [18]) but also by a single class of motors that work against the force produced by an optical trap [30]. The latter scenario is obviously very closely related to muscle contractility. In this chapter, we consider the latter scenario which is more relevant to muscle contractility, where the tug-of-war contest takes place between one class of similar motors working against an opposite load pulling at the end of the actin filament. In section 3.2 we discuss in more detail the observed increase in r with P , and show that this feature is directly related to Hill’s equation for muscle contraction. In sections 3.3 and 3.4 we present our model for sarcomere shortening, based on the system model described in section 1.5.1, and present our

computer simulations of muscle contraction. As will be shown, we find that the EMC effect leads to a polarized attachment probability along the actin filament, which might disrupt muscle performance. Interestingly, these feature becomes significant only in system whose size is larger than that of the sarcomere.

3.2 A simple derivation of Hill's equation

In this section we examine more closely the experimental results of ref. [34] regarding the increase in r with P . To this end, it is useful to define the dimensionless variables $0 \leq x \equiv P/P_0 \leq 1$, and $0 \leq y \equiv v/v_{\max} \leq 1$, where v_{\max} is the maximum contraction velocity at $P = 0$. When expressed in terms of these variables, Hill's equation (3.1) takes the dimensionless form:

$$y = \frac{1 - x}{1 + cx}, \quad (3.2)$$

where c is a constant. Notice that Eq. 3.2 satisfies both the relation that $y = 1$ for $x = 0$ (load-free contraction) and $y = 0$ for $x = 1$ (isometric contraction). The other important notion in relation to muscle contraction is the observed (see, e.g., Fig. 3(D) in ref. [34]) increase in r with P , which is well approximated by the linear relationship

$$r = r_0 + (r_1 - r_0)x, \quad (3.3)$$

where r_0 and r_1 denote the attachment probability for $x = 0$ and $x = 1$, respectively. To match the experimental data in ref. [34], we set $r_0 = 0.05$ and $r_1 \simeq 0.3$. From Newton's first law of motion, the fact that the sarcomere contracts at a constant velocity implies that the forces generated by the motors are balanced by the external load P and the friction forces in system. The latter originate from two sources: the surrounding medium and the attachment

of motors. The balance of forces reads

$$r(f_m - \lambda_m v) = \lambda v + \frac{P}{N}. \quad (3.4)$$

The expression in brackets on the left hand side of Eq. 3.4 can be identified as the force per motor

$$f_0(v) = f_m - \lambda_m v. \quad (3.5)$$

It includes a positive “active force”, f_m , and a negative “motor-friction force” characterized by the motor friction coefficient λ_m . On the right hand side of Eq. 3.4 we have the counter external load per motor P/N , and the friction force due to the viscous drag, λv ($\lambda \neq \lambda_m$), normalized per motor.

An interesting point, which to the best of our knowledge has not been recognized before, is the fact that Hill’s dimensionless equation (Eq. 3.2) can be derived from Eqs. 3.3 and 3.4 without any further assumptions. Explicitly, upon substitution of Eq. 3.3 in Eq. 3.4 and rearrangement of the resulting equation, one arrives to the following expression for the contraction velocity

$$v = \frac{f_m r_0 (1 - x)}{\lambda + \lambda_m [r_0 + (r_1 - r_0)x]}. \quad (3.6)$$

Also, for $P = 0$, Eq. 3.4 takes the form

$$\frac{f_m r_0}{v_{\max}} = \lambda + \lambda_m r_0. \quad (3.7)$$

Dividing Eq. 3.6 by v_{\max} , and using Eq. 3.7 as well as the relation $P/N = xP_0/N = x f_m r_1$,

one arrives to Eq. 3.2 with

$$c = \frac{\lambda_m(r_1 - r_0)}{\lambda + \lambda_m r_0}. \quad (3.8)$$

We further note that for $y = 1$ ($v = v_{\max}$), the following expression can be derived for f_0 if Eq. 3.7 is used in Eq. 3.5

$$f_0|_{y=1} = f_m \frac{\lambda}{\lambda + r_0 \lambda_m}. \quad (3.9)$$

The experimental data [34] gives $f_m = 6\text{pN}$, $f_0|_{y=1} = 4\text{pN}$, and $r_0 = 0.05$ which, upon substitution in Eq. 3.9, yields $\lambda_m = 10\lambda$. When this last result, together with the values for r_0 and r_1 are used in Eq. 3.8, one arrives to $c = 5/3$, which is within the range $1.2 < c < 4$ where the constant c is typically found for skeletal muscles [64]. Notice that we included viscous damping terms in our derivation which, as discussed earlier, is a matter of controversy. Nevertheless, it is important to recognize that Eq.(3.8) has a well defined limit when both λ and λ_m vanish, provided that λ/λ_m converges to a finite limit. The experimental results of ref. [34] seem to support the idea that the viscous forces are non-negligible.

3.3 System model

We now turn to our discussion on the relevance of the EMC effect to skeletal muscle contraction. To model muscle contraction we use the same model described in section 1.5.1 and add an external force P , that opposes the action of the motors, at the end of the elastic chain (i.e., the load P is applied on the N -th monomer of the chain). We set the distance between the monomers to $l \simeq 43/3 = 14.3$ nm, where the numerator is set by distance between collinear motor heads along the thick filament and the denominator comes from the fact that each thin filament is surrounded by three thick filaments [64]. As in our motility assay model presented in chapter 2, we use the term “attached” to refer to a motor head

that exerts force on the actin filaments at a given instance. In doing so, we adopt Huxley’s simple two-state scheme that only distinguishes between force-producing (“attached”) and non force-producing (“detached”) motors. As discussed above, more recent models expand this scheme by introducing more states (e.g., strongly and weakly attached states), but this expansion is not necessary for our purpose, which is to examine the relevance of the EMC effect to muscle contraction. Thus, we assume that a motor exerts a force of magnitude f_0 on the actin filament in the attached state, and no force in the detached state. The other model parameter is the attachment probability of the motors, r . As discussed above, both f_0 and r vary with v . We do not, however, consider the spatial (motor-to-motor) and temporal variations of r and f_0 at a given v . Thus, these two quantities represent the typical attachment probability and motor force, respectively. As we will demonstrate below, it is the EMC effect that leads to spatial variations in the *effective* (mean) attachment probability of the motors, $\langle r \rangle$. Strictly speaking, the bare attachment probability r in Eqs. 3.3 and 3.4 should be replaced with the effective attachment probability $\langle r \rangle$, which is, in fact, the experimentally measured quantity. However, as depicted later on, we find that the difference between the two is quite small in the case of muscle contraction.

3.4 Monte Carlo computer simulations

We study the system by using Monte Carlo simulations that include two types of elementary moves (as in the gliding assay simulations): one in which the state (connected or disconnected) of a randomly chosen motor changes, and the other in which two randomly chosen motors with opposite states change their states simultaneously. For each move attempt, the elastic energy E^{el} of the chain is recalculated, and the move is accepted or rejected according to the conventional Metropolis criterion with the statistical weights given by Eq. 1.3.

3.4.1 A Polarized attachment probability due to the EMC effect

In half sarcomere, each thick filament has about 150 motor heads [1]. To simulate muscles operating under conditions of optimal force generation, we assume that there is a full overlap between the thick and thin filaments [65], and consider a chain with $N = 150/2 = 75$ monomers (where the factor of 2 in the denominator originating from the 1:2 ratio between thin and thick filaments)¹. We also simulate larger systems of $N = 150$ and $N = 300$ nodes and fix the model parameters to $r = 0.05$, $f_0 = 6$ pN, and $k_s \simeq 4.5$ N/m². Our simulation results for the mean attachment probability, $\langle r(i) \rangle$, as a function of i ($1 \leq i \leq N$), the position of the monomer along chains, are depicted in Fig. 3.2 for $N = 75$ (A), $N = 150$ (B), and $N = 300$ (C). The simulations reveal that due to the EMC effect, the attachment probability becomes a monotonically increasing function of i . The origin of this feature is the fact that the springs are not equally stretched (as can be inferred from the derivation of the elastic energy in section 1.5.2). Generally speaking, attachment of a motor to a certain node i leads to a reduction in the energy of the springs with $j < i$. This reduction in the elastic energy makes statistically more favorable the configurations with polarized attachment of motors. For each N , there is a single node ($i = i^*$) where the attachment probability, $\langle r(i^*) \rangle$, is independent of P and takes a value which is very close to the bare attachment probability r . The difference between the attachment probabilities at both ends of the chain (i.e., for $i = 1$ and $i = N$) increases with both N and P . For $N = 75$, the variation in $\langle r(i) \rangle$ is quite small, becoming meaningful only at near-stall forces $P/(f_0N) \simeq 0.05$. In contrast, for

¹Due to the incommensurability between the motor heads and the actin binding sites there is, at each instance, a small fraction of motors that are practically unable to bind to the actin. Thus, the number of motors per filament in half sarcomere should be probably set to a somewhat smaller number ($N \sim 65$). We also ignore the fact that the length of the thin filament ($\sim 1 \mu\text{m}$) is larger than half the length of the thick filament ($\sim 0.8 \mu\text{m}$), which means that, even at full overlap, the external force is applied a certain distance away from the position of the nearest motor head. Introducing these features into the simulations does not alter significantly our results.

²The spring constant is given by $k_s = YA/l$, where Y is the filament Young's modulus, A the cross sectional area, and l the distance between motors. The Young's modulus of the thick filament is similar to that of the thin filament, $Y_{\text{thick}} \sim Y_{\text{thin}}$. However, $A_{\text{thick}} \sim 10A_{\text{thin}}$, and $l_{\text{thick}} = 0.5l_{\text{thin}}$ (due to the 2:1 number ratio between them). Thus, $k_{s-\text{thick}} \gg k_{s-\text{thin}}$, which means that to a very good approximation the compliance of the thick filament can be ignored.

$N = 150$, the variations in $\langle r(i) \rangle$ are significant and may be as large as $\langle r(N) \rangle / \langle r(1) \rangle \gtrsim 4$. The mean attachment probability, $\langle r \rangle \equiv [\sum_{i=1}^N \langle r(i) \rangle] / N$, is plotted in Fig. 3.2(D) as a function of $P / (f_0 N)$. For both $N = 75$ and $N = 150$ and for all values of P , we find that $\langle r \rangle \simeq r$, which shows that the decrease in $\langle r(i) \rangle$ for $i < i^*$ is almost offset by the increase in $\langle r(i) \rangle$ for $i > i^*$. This is not the case for $N = 300$, where $\langle r \rangle$ exhibits a steady increase with P . The increase in $\langle r \rangle$ is due to the fact that at large forces (notice that the applied loads are proportional to N), the attachment probability $\langle r(i) \rangle$ becomes a rapidly increasing function of i . The implication of the rise in $\langle r \rangle$ is that the stall force *per motor* increases to $\simeq 0.1 f_0$ (from $\simeq 0.05 f_0$ for $N = 75$ and $N = 150$), which explains why in Fig. 3.2(D), the range of forces simulated for $N = 300$ is larger than for $N = 75$ and $N = 150$.

3.4.2 Sarcomere shortening simulations

The above results seem to indicate that for $N > 75$, the variations in $\langle r(i) \rangle$ may be sufficient to disrupt muscle performance. However, one needs to recall that the simulation results depicted in Fig. 3.2 correspond to fixed values of r and f_0 , while in reality the values of these quantities vary with the shortening velocity v . To correctly evaluate the significance of the EMC effect in muscle contraction, one needs to run simulations where for each value of P , the appropriate value of v is chosen and, accordingly, the values of r and f_0 are set. This is done by using Eqs. 3.2, 3.3 and 3.5. Specifically, for a given value of y , the value of x is determined from Hill's Eq. 3.2

$$y = \frac{1 - x}{1 + (5/3)x}, \quad (3.10)$$

while the value of f_0 is set according to Eq. 3.5

$$f_0 = 6(1 - \frac{y}{3}) \text{ [pN]}. \quad (3.11)$$

The determination of r is slightly more complicated. The complication arises due to the

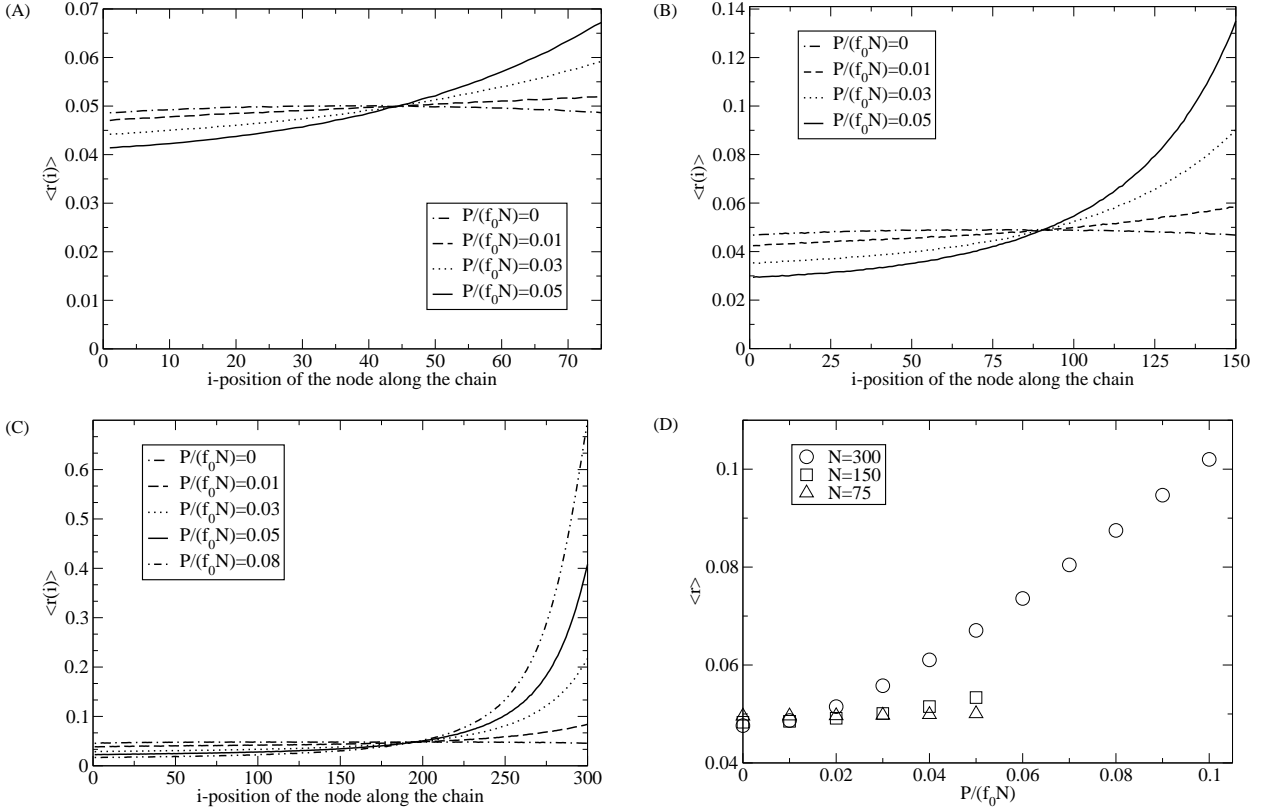


Figure 3.2: The attachment probability $\langle r(i) \rangle$ to the i -th chain node, calculated for chains consisting of (A) $N = 75$, (B) $N = 150$, and (C) $N = 300$ nodes. For each N , the attachment probability is plotted for various values of the load P . (D) The effective attachment probability $\langle r \rangle$ as a function of the dimensionless load per motor $P/(f_0 N)$ for $N = 75$ (triangles), $N = 150$ (squares), and $N = 300$ (circles).

fact that the bare attachment probability r appearing in Eqs. 3.3 and 3.4 should be replaced with the effective attachment probability, $\langle r \rangle$, which is the experimentally measured quantity and which is not known a-priori. Therefore, for each value of y we simulated different values of r and, using linear interpolation, determined the value of r that yields the desired $\langle r \rangle$.

Our results for the sarcomere simulations are summarized in Fig. 3.3 which shows the position-dependent attachment probability, $\langle r(i) \rangle$, calculated for a chain of size $N = 75$ and for different loads. It is important to note that in the simulations presented in Fig. 3.2 the motor force is taken as $f_0 = f_m = 6$ pN, while the spring constant $k_s = 4.5$ N/m. This means that at physiological temperature of $T = 310K$, $\beta^* \simeq 10^{-3}$, which is the value of

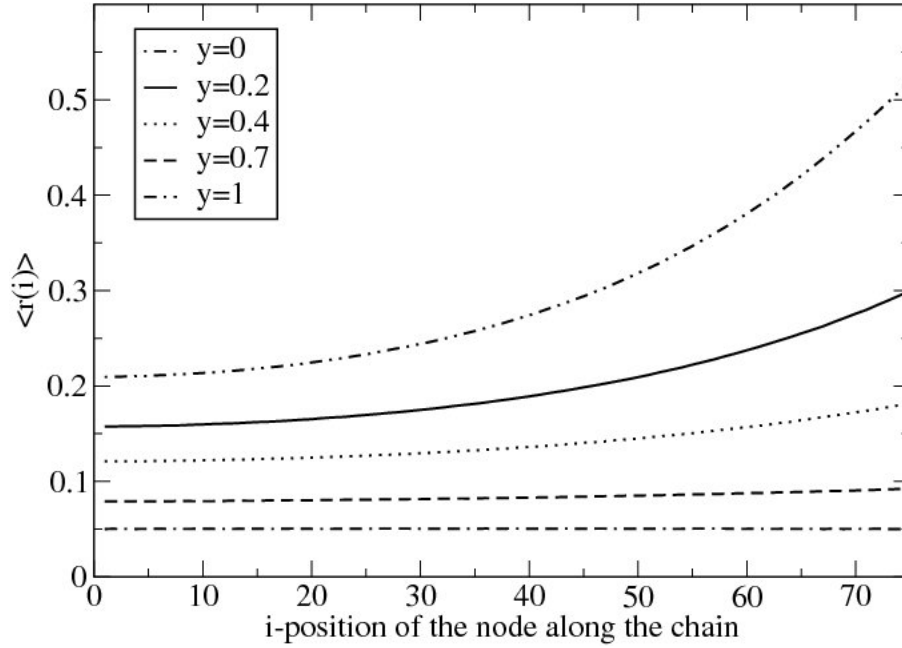


Figure 3.3: The attachment probability $\langle r(i) \rangle$ to the i -th chain node, calculated for different values of the rescaled velocity y .

β^* used in the simulations depicted in Fig. 3.2. In Fig. 3.3, we use the above Eq. 3.11 to evaluate f_0 . This means that for each curve in Fig. 3.3, the dimensionless parameter β^* has been redefined to $\beta^* = 10^{-3}(1 - y/3)^2$.

Similarly to the results plotted in the above Fig. 3.2(A), the results depicted in Fig. 3.3 indicate that for $1 \leq i \leq N = 75$, $\langle r(i) \rangle$ remains fairly uniform for high and medium velocities and that, consequently, the difference between r and $\langle r \rangle$ is quite small. This observation is consistent with the idea that at high and medium velocities v , the detachment of motors occurs after the completion of the power stroke. The associated detachment rate, which can be estimated by $\tau_{\text{det}}^{-1} \sim v/\delta$, where δ is the step size ($\delta \sim 6$ nm) which is the same for all the motors [34]. This picture is relevant only for high and medium velocities where the motors attach, execute the power stroke, and then unbind. At very low velocities ($y \simeq 0$) close to the isometric load ($x \simeq 1$), the motors may detach and reattach multiple times before the power stroke is completed [66]. The number of attachments per power stroke need not be the same for all the motors and, therefore, variations in the attachment probabilities [which are indeed observed in Fig. 3.3(B) at small values of y] can be tolerated in this limit without

negative consequences for muscle contractility.

3.5 Summary

In this chapter we examined the thoroughly studied problem of muscle contraction in light of the growing interest in collective dynamics of motor proteins. The basic contractile unit of the muscle is the sarcomere which appears to have almost the same length in different muscle cells of different vertebrates. We argue that the origin of this remarkable feature of muscle cells may be the *elasticity-mediated crosstalk* (EMC) effect, which is related to the changes in the attachment/detachment rates of the myosin II motors in response to the tensile stress that they (collectively) generate in the F-actin. The associated changes in the duty ratio of the motors can impair their ability to cooperate efficiently during muscle contraction. Specifically, the major problem originating from the EMC effect is that it leads to an increase in the attachment probability of motors located near the Z-line while, simultaneously, decreasing the attachment probability of the motors in the central part of the sarcomere (M-line). The resulting variations in the duty ratios of the motors along the thick filament pose a serious problem in light of the fact that the detachment rate of the motors is primarily a function of the step size and the muscle shortening velocity and, therefore, should be fairly uniform. Using computer simulations of a simple bead-spring model we demonstrated that this undesired effect can be almost neglected for half-sarcomeres consisting of less than approximately $2N = 150$ motors. Remarkably, this is precisely the “universal” size of half a sarcomere in muscle cells across vertebrates.

Another notable result of our study is the derivation of the celebrated Hill’s equation for the muscle force-velocity relationship. The basic assumptions in our derivation are given by Eqs. 3.3 and 3.4. The former describes the experimentally measured linear relationship between the attachment probability and the load, while the latter is simply Newton’s first law for an object (the actin filament in this case) moving at constant velocity. As a bonus,

we obtain an expression relating the constant c in the dimensionless form of Hill's equation to some of the system parameters.

Chapter 4

Discussion

Motor proteins are a key component in virtually all eukaryotic cells. They are involved in various important biological processes such as cell division and muscle contraction. Over the past years, our knowledge concerning how these molecules operate and interact with the cytoskeletal filament has increased dramatically, as a result of theoretical studies and improved experimental techniques. Recently, there has been an increased interest in the collective action of motor proteins, particularly in the way that cooperative effects change their duty ratios. One notable example is the elasticity-mediated crosstalk (EMC) coupling between myosin II motors, whose origin is the tensile stress that they collectively generate in actin filaments. The EMC effect was originally proposed in order to explain the observed distribution of reversal times in motility assays of myosin II motors and actin filaments with alternating polarities [18]. Such filaments exhibit bidirectional motion due to the action of motors exerting opposite forces on actin segments with opposite polarities. The “tug-of-war” between the two antagonistic motor parties leads to large stress fluctuations along the elastic actin track. As a result, the motors change their attachment/detachment statistics in order to relieve the strain energy in the filaments. More specifically, during bidirectional motion, the motors duty ratio decreases and, on average, each one of them becomes effectively less processive. The EMC between motors in bidirectional motion, thus, is a collective effect that

decreases their degree of cooperativity.

The aforementioned motility assay for bidirectional motion constitute a rather unusual experimental setup. In this thesis we explored the role of the EMC effect in two more common scenarios. The first one is that of conventional motility gliding assays where myosin II motors work on polar actin filaments. In this case, the filaments move unidirectionally because all the motors exert forces in the same direction. Unlike in the “tug-of-war” case, the force fluctuations along the filament are limited when all the forces are applied in the same direction and, therefore, the EMC effect is expected to be quite small. Our statistical mechanical analysis of this problem, presented in chapter 2, demonstrates this point. The magnitude of the EMC effect is quantified by introducing the dimensionless parameter β^* [see Eq. 1.12] that characterizes the ratio between the typical elastic energy per actin segment and the thermal energy. Our analysis reveals that the *effective* attachment probability $\langle r \rangle$ of non processive myosin II motors drops linearly with $\sqrt{\beta^*}$ (see Eq. 2.20) from the value of r , the *bare* attachment probability, at $\beta^* = 0$ (i.e., for an infinitely rigid filament that does not exhibit EMC). Our calculation holds for small values of β^* , which is indeed the case for actomyosin motility assays where $\beta^* \sim 0.002$. This means that in this conventional actomyosin gliding assays the EMC effect has only a small impact on the attachment probability of the motors, i.e. $\langle r \rangle \simeq r$.

The second system under investigation in this thesis is skeletal muscles. As in the case of the motility assays for bidirectional motion, this system features a tug-of-war competition between opposite forces. But while in bidirectional motion two motor parties work against each other, in the case of muscle contraction, the tug-of-war takes place between the motors and an external opposite force that pulls at the end of the sarcomere. This type of tug-of-war also creates larger stress fluctuations along the actin track, specifically near the end where the external force is applied. Our analysis of this system, presented in chapter 3, reveals that the stress fluctuations can be reduced by inhomogeneous attachment of the motors. Specifically, the motors will tend to attach at a higher (lower) rate close to (away from) the

end of the sarcomere where the external load is applied. In other words, the EMC leads to a polarized attachment probability, where the motors in proximity to the last monomer attach with higher probability than motors far away from this point. The problem with this observation, however, is that the duty ratio variations between motors may seriously impair their ability to efficiently cooperate with each other (see discussion in chapter 3). Nevertheless, we find that the polarization of the attachment probability becomes significant either when a large external force is applied, or when the system size is larger than the “universal” size of sarcomeres in vertebrates (i.e., $N > 75$). Thus, our analysis proposes a possible solution for the long standing puzzle concerning the similarity of the sarcomere length in different species in nature. Recent advances in single molecule techniques [67] open the opportunity for testing our theoretical predictions concerning the polarization of the attachment probability. Specifically, optical tweezers provide the mean to apply piconewton forces against the gliding motion of the thin filament, while the duty ratio may be directly measured using high resolution atomic force microscopy (AFM).

Motor proteins are the “engines of biology”, converting chemical energy into mechanical work. To gain a better understanding of their action, one needs to develop models that integrate and couple the biochemical cycle of these molecules with their mechanical features and with the elasticity of the associated cytoskeletal filaments. Over the past century, this problem has drawn attention from different scientific disciplines. One of the main issues that has been largely debated within the community is the role of friction forces in the process of muscle contraction. Some theoretical studies support the notion that friction forces play a minor role in muscle contraction, while others argue that friction is a non-negligible force that may emerge from the medium surrounding the filaments and / or the motors themselves. Our simple derivation of Hill’s equation (see section 3.2) interprets the experimental findings in ref. [34] as if friction forces are indeed non-negligible (see Eq. 3.4). Nevertheless, it is important to emphasize that our approach does not rely on this notion. What we have presented in this thesis is a unique statistical mechanical approach for investigating the

collective action of myosin II motors. Our theoretical approach bypasses the aforementioned controversies by introducing only two variables that do not depend on friction at all, namely the duty ratio r and the dimensionless energy β^* . The resulting EMC effect can be easily integrated into other theoretical model. Specifically, with the steady improvement in imaging techniques and computer modeling, more atomistic models for muscles may be "just around the corner".

Bibliography

- [1] B. Alberts, D. Bray, J. Lewis, M. Raff, K. Roberts, and J. D. Watson, *Molecular Biology of the Cell* (Garland, New York, 1994).
- [2] E. Mandelkow and E.M. Mandelkow, *Curr. Opin. Struct. Biol.* **4**, 171 (1994).
- [3] K.J. Palmer, P. Watson and D.J. Stephens, *Biochem. Soc. Symp.* **72**, 1 (2005).
- [4] B. A. Rowning et. al., *Proc. Natl. Acad. Sci.* **94**, 1224 (1997)
- [5] K. Bloom, *Curr. Biol.* **3**, R430 (2003).
- [6] T.P. Stossel, *Sci. Am.* **271** 54 (1994).
- [7] B. Feierbach and F. Chang, *Curr. Opin. Microbiol.* **4**, 713 (2001).
- [8] D.A.D. Parry and P.M. Steinert, *Intermediate Filament Structure* (Springer-Verlag, New York, 1995).
- [9] J. Howard, *Mechanics of Motor Proteins and the Cytoskeleton* (Sinauer, Sunderland MA, 2001).
- [10] H. Higuchi and S. A. Endow, *Curr. Opin. Cell Biol.* **14**, 50 (2002).
- [11] H. B. McDonald, R. J. Stewart and L. S. Goldstein, *Cell* **63**, 1159 (1990).
- [12] M. Schliwa, *Nature*, **401**, 431 (1999).
- [13] H. Miki, Y. Okada, and N. Hirokawa, *Trends. Cell Biol.***15**, 467 (2005).

- [14] L. M. Coluccia (ed.), *Myosins: A Superfamily of Molecular Motors* (Springer, Dordrecht, 2008).
- [15] Cooper G.M. *The Cell: A Molecular Approach. 2nd edition* (Sinauer Associates, Sunderland, MA, 2000).
- [16] M. LeMasurier and P. G. Gillespie, *Neuron* **48**, 403 (2005).
- [17] H. A. AL-Khayat, L. Hudson, M. K. Reedy, T. C. Irving and J. M. Squire, *Biophys. J.* **85**, 1063 (2003).
- [18] B. Gilboa, D. Gillo, O. Farago, and A. Bernheim-Groswasser, *Soft Matter* **5**, 2223 (2009).
- [19] F. Jülicher and J. Prost, *Phys. Rev. Lett.* **75**, 2618 (1995).
- [20] F. Jülicher and J. Prost, *Phys. Rev. Lett.* **78**, 4510 (1997).
- [21] M. Badoual, F. Jülicher, and J. Prost, *Proc. Natl. Acad. Sci. USA* **99**, 6696 (2002).
- [22] M. O. Magnasco, *Phys. Rev. Lett.* **71**, 1477 (1993).
- [23] A. Ajdari, D. Mukamel, L. Peliti and J. Prost, *J. Phys. I* **4**, 1551 (1994).
- [24] R. D. Astumian and M. Bier, *Phys. Rev. Lett.* **72**, 1766 (1994).
- [25] J. E. Molloy, J. E. Burns, J. Kendrick-Jones, R. T. Tregear, and D. C. S. White, *Nature* **378**, 209 (1995).
- [26] J. T. Finer, R. M. Simmons, and J. A. Spudich, *Nature* **368**, 113 (1994).
- [27] H. Higuchi, T. Yanagida, and Y. E. Goldman, *Biophys. J.* **69**, 1000 (1995).
- [28] H. Kojima, A. Ishijima, and T. Yanagida, *Proc. Natl. Acad. Sci. USA* **91**, 12962 (1994).
- [29] K. C. Holmes, D. Popp, W. Gebhard, and W. Kabsch, *Nature* **347**, 44 (1990).

- [30] S. L. Hooper, K. H. Hobbs, and J. B. Thuma, *Prog. Neurobiol.* **86**, 72 (2008).
- [31] H. E. Huxley, A. Stewart, H. Sosa, and T. Irving, *Biophys. J.* **67**, 2411 (1994).
- [32] K. Wakabayashi, Y. Sugimoto, H. Tanaka, Y. Ueno, Y. Takezawa, and Y. Amemiya, *Biophys. J.* **67**, 2422 (1994).
- [33] T. L. Daniel, A. C. Trimble, and P. B. Chase, *Biophys. J.* **74**, 1611 (1998).
- [34] G. Piazzesi, et. al., *Cell* **131**, 784 (2007).
- [35] M. J. I. Müller, S. Klumpp, and R. Lipowsky, *Proc. Natl. Acad. Sci. USA* **105**, 4609 (2008).
- [36] T. A. J. Duke, *Proc. Nat. Acad. Sci. USA* **96**, 2770 (1999).
- [37] K. Kruse and D. Riveline, *Curr. Top. Dev. Biol.* **95**, 67 (2011).
- [38] T. Guérin, J. Prost, P. Martin, and J.-F. Joanny, *Curr. Opin. Cell Biol.* **22**, 14 (2010).
- [39] S. Banerjee, M. C. Marchetti, and K. Müller-Nedebock, *Phys. Rev. E.* **84**, 011914 (2011).
- [40] T. J. Burkholder, R. L. Lieber, *J. Exp. Biol.* **204**, 1529 (2001).
- [41] H. E. Huxley, *Science* **164**, 1356 (1969).
- [42] A.V. Hill, *Proc. R. Soc. London B Biol. Sci.* **126**, 136 (1938).
- [43] R. V. Mastrigt, *IEEE Trans. Biomed. Eng.* **27**, 413 (1980).
- [44] A. F. Huxely, *Prog. Biophys. Biophys. Chem.* **7**, 255 (1957).
- [45] H. E. Huxley, *J. Mol. Biol.* **7**, 281 (1963).
- [46] J. Kendrick-Jones, W. Lehman, A. G. Szent-Gyorgyi, *J. Mol. Biol.* **54**, 313 (1970).
- [47] R. W. Lymn, E. W. Taylor, *Biochemistry* **10**, 4617 (1971).

- [48] B. R. Munson, D. F. Young, T. Okiishi, W. W. Huebsch *Fundamentals of Fluid Mechanics* (Wiley, Hoboken NJ, 2010).
- [49] D. Bernstein, Phys. Rev. E. **71**, 041103 (2005).
- [50] A. F. Voter *Radiation Effects in Solids* (Springer, Dordrecht, 2005).
- [51] G. Lan, X. Sun, Biophys. **88**, 1407 (2005).
- [52] K. Kitamura, M. Tokunaga, S. Esaki, A.H. Iwane, T. Yanagida, Biophysics **1**, 1 (2005).
- [53] S. Walcott, S. X. Sun, Phys. Chem. Chem. Phys. **11**, 4871 (2009).
- [54] A. Mansson, Biophys. J. **98**, 1237 (2010).
- [55] L. Marcucci, L. Truskinovsky, Eur. Phys. J. E. **32**, 411 (2010).
- [56] B. Chen, H. Gao, Biophys. J. **101**, 396 (2011).
- [57] S. J. Kron, J. A. Spudich, Proc. Natl. Acad. Sci. USA **83**, 6272 (1986).
- [58] C. R. Worthington, Nature **193**, 1283 (1962).
- [59] G. F. Elliott, C. R. Worthington, Int. J. Biol. Macromol. **29**, 213 (2001).
- [60] A. R. Bausch, W. Möller, E. Sackmann, Biophys. J. **76**, 573 (1999).
- [61] K. Keren, P. T. Yam, A. Kinkhabwala, A. Mogilner, J. A. Theriot, Nat. Cell Biol. **11**, 1219 (2009).
- [62] A. Landesberg, S. Sideman, Am. J. Physiol. **278**, H1274 (2000).
- [63] D. Hexner, Y. Kafri, Phys. Biol. **6**, 036016 (2009).
- [64] Y. C. Fung, *Biomechanics: Mechanical Properties of Living Tissues* (Springer-Verlag, New York, 1993).

- [65] J. Keener, J. Sneyd, *Mathematical Physiology*, (Springer-Verlag, New York, 1998).
- [66] M. Linari, M. Caremani, V. Lombardi, Proc. R. Soc. B. **277**, 19 (2010).
- [67] C. Veigel, C. F. Schmidt, Nat. Rev. Mol. Cell Biol. **12**, 163 (2011).